Geochronology and tectonic setting of voluminous granitoids and related rocks and associated extensional structures in Dronning Maud Land (East Antarctica)

Amel Eldrdery Suliman

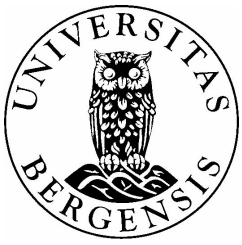

Department of Earth Science
The Faculty of Mathematics and Natural Sciences
University of Bergen, Norway
2011

Geochronology and tectonic setting of voluminous granitoids and related rocks and associated extensional structures in Dronning Maud Land (East Antarctica)

Amel Eldrdery Suliman

This thesis is submitted in partial fulfilment of the requirements for the degree of Master of Geodynamics at the University of Bergen.

Department of Earth Science
The Faculty of Mathematics and Natural Sciences
University of Bergen, Norway
2011

Abstract

The history of the tectonic evolution in central Dronning Maud Land (cDML), East Antarctica can be inferred from various zircon grains for U-Pb zircon age determination with the Laser-Ablation Inductively-Coupled-Plasma Mass Spectrometry (LA-ICP-MS) technique. The zircons grain of the different rocks collected from different geographic location in cDML include the Shcherbakova area, the Holtedahlfjella and Zwiesel area. New zircon U-Pb ages have been used to establish relationships between ancient rocks, to obtain new insights into the Early Paleozoic orogenic collapse and contemporaneous voluminous late-tectonic intrusions in central Dronning Maud Land. Most of these results agree reasonably well with the supercontinent assemblage chronology of Gondwana within the cDML. The oldest ages of 1100 Ma to 910 Ma correspond to the final construction of the Rodinia. The ages of 900 Ma to 620 Ma are likely to represent a number of rifting events that are associated with the destruction of Rodinia. The U-Pb zircon ages of 610 Ma to 535 Ma corresponds with the re-assemblage of parts of E and W- Gondwana during the East-African orogeny. The youngest ages of 530 Ma to 458 Ma correspond to the Pan-African orogeny and thus the final amalgamation of Gondwana. Grenville-age rocks of ~ 1100Ma represent the oldest basement yet found in cDML that was during large-scale delamination intruded by the late-tectonic granitoids. A detrital zircon age of 950-680 Ma found in one sample of the cDML is reported from this area outside of the Schirmacher Oasis for the first time in this study.

Key words: central Dronning Maud Land, East Antarctica, East Gondwana, West Gondwana, granitoids, amphibolite facies metamorphism, granulite facies metamorphism, Pan-African and Neoproterozoic-Cambrian times.

Table of contents:

ACRONYMS

ANS	Arabian-Nubian Shield
CDML	Central Dronning Maud Land
CL	Cathodoluminescence
EAAO	East-African Antarctic orogen
J	Jacobs
JJ	Joachim Jacobs
LA-ICPMS	Laser-Ablation Inductively-Coupled-Plasma Mass Spectrometry
MB	Mozambique Belt
MSWD	Mean Square Weighted Deviation
SHRIMP	Sensitive High Resolution Ion Microprobe
TIMS	Secondary Ion Mass Spectrometry
Zrc	Zircon

ACKNOWLEDGMENT

My great thanks to Department of Earth Science, Faculty of Mathematics and Natural Sciences, University of Bergen, for giving me opportunity to pursue my study. I would like also thank to the stastens Lånekassen, Norway, for the financial support.

I greatly appreciate to my main supervisor Prof. Joachim Jacobs, for his tireless efforts and guidance's through all stages of my study, also to thanks him for giving me a great project, and for providing me with samples and thin sections. I would like to acknowledge my co-supervisors Prof. Jan Kosler and Dr. Ilka Kleinhanns, for their advices, helpings and encouragements. I also thank to Siv Hjorth who helped me with my samples analyses in the ICP-MS lab. I show gratitude to Egil Erichsen who helped me with my Cathodoluminescence images. I thank to Marile Andersson who helped me with preparing lab. I greatly thank to Kosuke Ueda, for being there with his advice and helps. I also thank to Anna Ksienzyk and Dr. Fabian Kohlmann. Great thanks to Department of Earth Science members, especially Caroline Ertsås.

I am greatly appreciating to Dr. Salah Basheeri and Prof. Abd Alhalim Alnadee, Department of geology, Faculty of science, university of Khartoum, Sudan, for giving me the opportunity to be in the field of scientific research. Additionally I thank to A, Shama, Dr. Ensaf, Dr. Fath Albreer, Dr. Samia, Dr. Ebrahim and Dr. Amanee, for encouragements.

I appreciate my collogues; Kurnia Juli Utami, Irina Maria Dumitru, Helge Jorgensen, Karen Johannessen, Espen Torgersen and Anette Broch, at Department of Earth Science,

University of Bergen, for a nice group work and for helpful discussion and great moments.

I would like also to express my thankful to the Sudanese friends in Bergen; Hiba, Sara, Wijdan, and Gada, for all wonderful times we have shared. I also thank to Dr. Howiada and Wadia, for helping me and give me good advices.

I would like to convey my heart felt appreciation to my family, my great mother Noor Alhwda, my Aunt Nafessa, my sister Mysoon, and my cousins Ayman, Eman and Mogbeel, for their encourages and supports. Special thanks to my husband Ehab for his care, continuous love, endless support and encouragements, which enabled me to complete this work. My thanks extend to my mother in law, my sisters in law and my brothers in law.

Introduction

1.1 Research objective and previous work

In this study, zircons were dated with the Laser-Ablation Inductively-Coupled-Plasma Mass Spectrometry (LA-ICPMS) method to determine the age of granitoids and related rocks within East Antarctica. Six samples were selected from different localities in central Dronning Maud Land (cDML), East Antarctica (Fig. 1) to further constrain the tectonic history of A2-type granitoids and basement rocks of DML. The studied sample suite comprises metamorphic rocks (hornblende gneiss and amphibolites from the Shcherbakova area, grey gneiss from the Holtedahlfjella) and granitoids (biotite-hornblende granite from the Holtedahlfjella, charnockite and syenite from the Zwiesel area). Dronning Maud Land went through several major deformation events: (i) formation of Rodinia at ca. 1200 Ma (Grenville-age), (ii) destruction of Rodinia at 800-700 Ma, (iii) formation of Gondwana from 650 Ma to 520 Ma and (iv) final stage of Gondwana assembly from 520 Ma to 480 Ma. The formation of Gondwana is characterised by collision of East (Africa and South-America) and West (India, East-Antarctica and Australia) Gondwana leading to the so-called Pan-African orogeny around 500 Ma. The resulting suture zone is more than 9000 km long, strikes in N-S-direction and is called the East-African Antarctic orogen (EAAO) (Figure 1). The EAAO shows a strong lateral variation with abundant A-type granitoids in its southern part (present Mozambique and Antarctica) that are the focus of this study and compared with their source rocks, i.e. the basement. The granitoids are typically peraluminous to metaluminous and subalkaline in composition. They probably crystallized at mid-crust levels during orogenic collapse and subsequent extension. Heat input to trigger granitoid magmatism is thought to result from delamination of the lithosphere root (Jacobs et al., 2008).

First studies of the central DML have been performed since1960 by Russian, Indian and East German geologists focusing on the Wohlthatmassivet, Orvinfjella and the Mühlig-

Hofmannfjella. These studies provide some excellent petrological, structural and geochemical data by (Ravich and Solov'ev, 1966; Ravich and Kamenev, 1972; Kamenev et al., 1990). During the 90ies the area came into focus again by Indian and German geologists (Joshi et al., 1991; Bohrmann and Fritzsche, 1995; D'Souza et al., 1996). But they aren't get geochronological data (U-Pb zircon) to describe the tectono-thermal evolution of the basement, (e.g. Mikhalsky et al., 1997). More recently, a number of geochronological results has been published (Jacobs et al., 1998; Paulsson and Austrheim, 2003; Jacobs et al., 2003a-b) that show that most of the exposed crust of cDML is of Grenvillian (~1200 Ma) age and was widely modified and reworked during the Pan-African orogeny (600–500 Ma). The oldest rocks in cDML yet found is represented by the grenvillian-age basement comprising a thick sequence of metaigneous and sedimentary rocks with banded orthogneisses, metapelites, metapsammites, calcsilicates, pyroxene granulites and amphibolites. The banded orthogneiss is interpreted as representing a bimodal volcanic sequence. Oldest ages found in these rocks are around 1150–1100 Ma (Jacobs et al., 2003a-b) and a high grade metamorphic overprint is dated to the range of 1090-1050 Ma. During the Pan-African orogeny, associated with collision of East and West Gondwana about 550 Ma, the basement rocks were re-metamorphosed (Jacobs et al., 1998; Markl et al., 2003). The magmatic activity seems to continue during the entire period and climaxed with the construction of a post-collision extensional regime (530–510 Ma), which led to the creation of large volumes of granitic and syenitic rocks (Jacobs et al., 2003a-b). The formation of EAAO can be separated into two major periods; the first period (Pan-African I) occurred 560–550 Ma, and is characterized by upper amphibolite to granulite-facies. The second Period (Pan-African II), was between 520 and 480 Ma, and characterized by magmatic intrusions (Jacobs et al., 2008).

1.2 Study area

The study area is situated in central Dronning Maud Land (cDML) within E-Antarctica (Fig.3). The central Dronning Maud Land (cDML) includes the Wohlthatmassivet, Orvinfjella and the Mühlig-Hofmannfjella, where the samples analysed in this study are located. DML represents the southern part of the Late Neoproterozoic–Early Palaeozoic East African–Antarctic Orogen (EAAO) (Jacobs et al., 2008) and was formed during the the E and W Gondwana continent-continent collision. The EAAO shows a strong lateral variation with the northern part dominated by accretionary processes visible within the Arabian-Nubian Shield (ANS) and the southern part dominated by continent-continent collision. Within the southern part additionally high numbers A-type granitoids are described that point to different crustal regimes operating in these two parts. The Lurio Belt in Mozambique separates these two regimes of the EAAO (Jacobs et al., 2003a-b) (Fig.1).

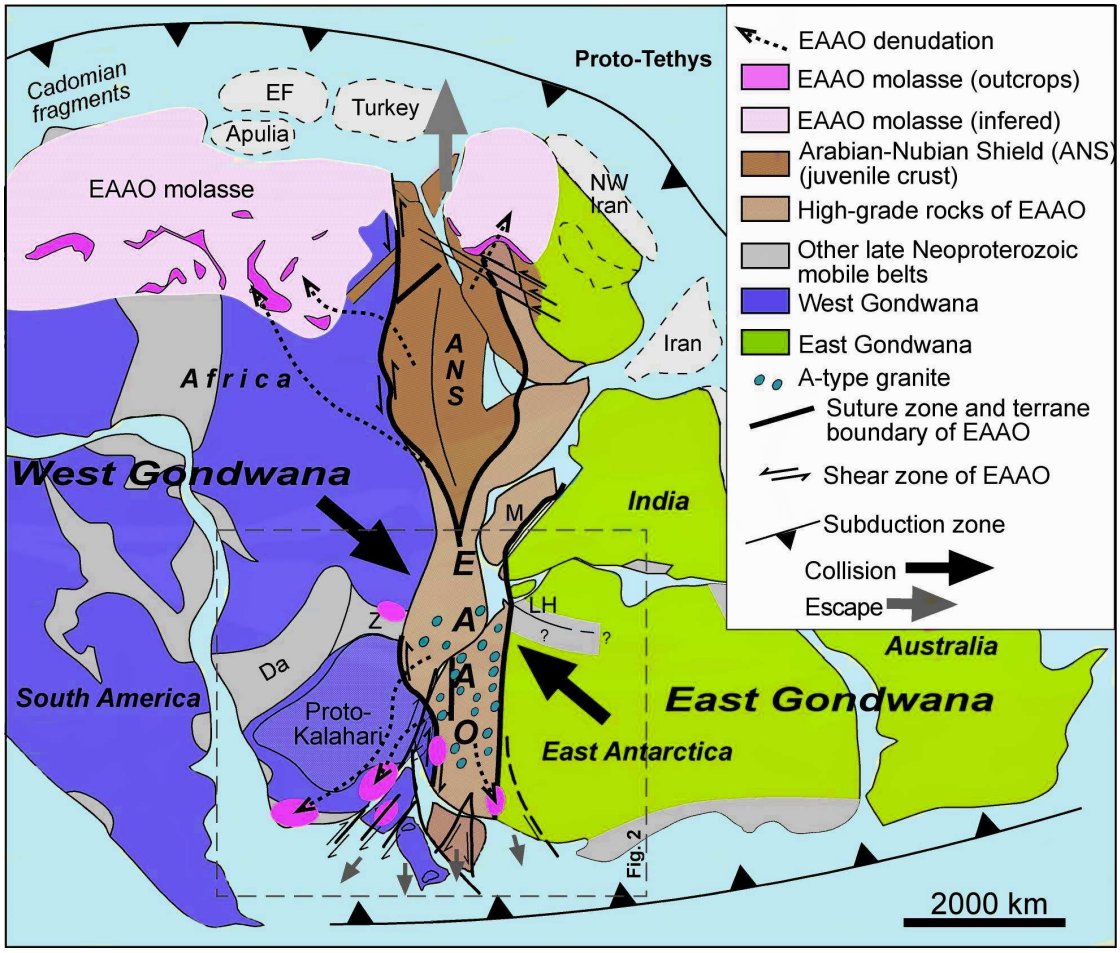

Fig. 1: The East African–Antarctic orogen (EAAO) was formed when the parts of proto–East and West Gondwana collided to form Gondwana. Abbreviations: ANS—Arabian-Nubian shield; Da—Damara belt; EF— European fragments; LH— Lützow-Holm Bay; M—Madagascar; Z—Zambesi belt after Stern (1994) & Jacobs and Thomas, (2004)

1.3 Method

Six samples (J1684, J1756, J1759, J1772, J1821, and J1825) from late-to post-tectonic rocks of central Dronning Maud Land, East Antarctica were examined in this study. Zircon grains of these samples were analyzed by Laser ablation inductively coupled plasma mass spectrometry (LA-ICP-MS) at department of Earth Science at University of Bergen (February 2011) and U-Pb ages were calculated to further constrain their geodynamic history. Sample locations and their lithology lists are shown in (Fig.2).

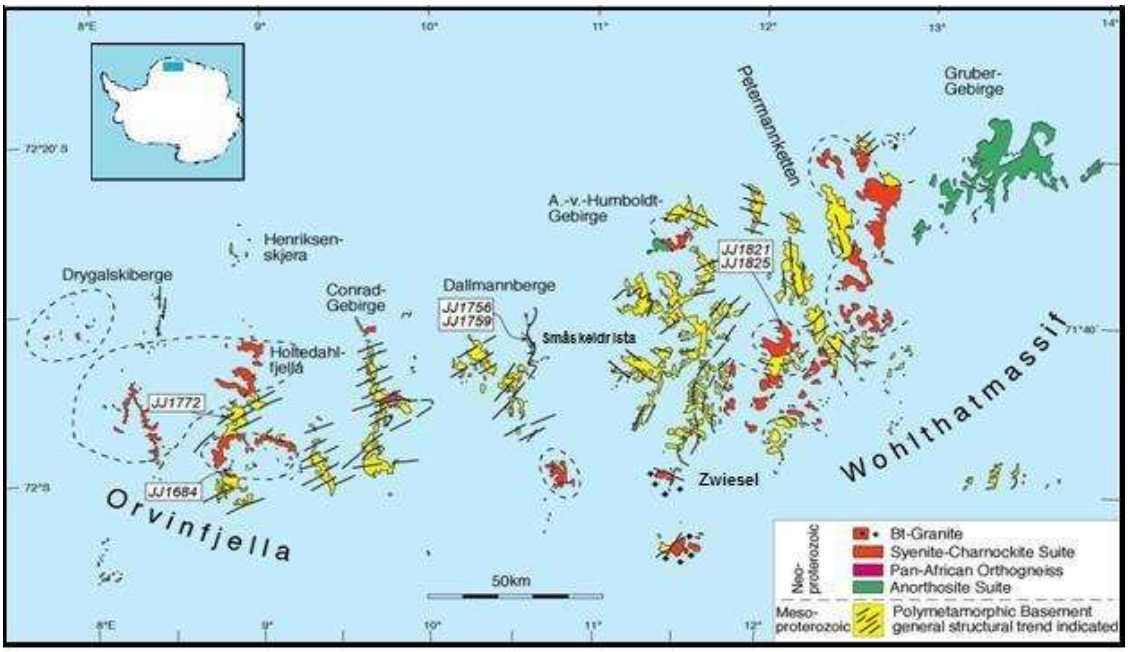

Fig. 2: geological map of central Dronning Maud Land, East Antarctica, showing the location of the analyses samples of this study

2. Regional geology

The evolution of the East African–Antarctic orogen (EAAO resulted from the collision between various parts of East Gondwana (consisting of Antarctica, Australia, and India) and West Gondwana (consisting of Africa and South America) during late Neoproterzoic times until early Paleozoic times (Jacobs et al., 2008). Within the EAAO many lithotectonic units consisting of similar rock assemblages show the same complex deformational history with large thrust sheets or nappes.

The Mozambique Belt and Dronning Maud Land represent the southern part of EAAO that was formed by continent-continent collision (Jacobs et al., 2008). The Arabian-Nubian Shield represents the northern part of EAAO that was formed as a result of the accumulation of island arcs terranes. The northern and southern parts are divided by the E-W-trending Lurio belt (present Mozambique). Pan-African granitoids are abundant in the southern part whereas they are absent in the northern part. Formation of the high grade metamorphism rocks (granulite-facies metamorphism 700 and 550 Ma), related to the crustal thickening, associated with recumbent folds, flowed by late- to post-tectonic Cambrian magmatic province c. 530 and 485 Ma is known in the southern part of the EAAO, included minor gabbro intrusions c. 530-520 Ma, followed by the main charnockite-granitoid magmatic event c. 510- 500 Ma.

The A2-type granitoids were emplaced at mid-crustal levels during collapse and extension of the orogeny (Jacobs et al., 2008) probably triggered by delimitation of the lithosphere root. The migmatization presumably resulted from water entering the system of dry and hot granulite conditions deep in the crust or by uplift of dry granulite into upper crustal levels. The latter possibility is more reasonable since PT constraints for retrogression show low pressure and temperature estimated from the co-existing mineral pairs in the migmatite and the temperature from rim composition of the garnets in the granulite.

2. 1 Geological setting

2.1.1The East African Antarctic Orogen (EAAO)

The ENE-WSW trending Lurio Belt divides EAAO into two different crustal segments. The southern part of EAAO, in the Dronning Maud Land in East Antarctica, comprises high grade metamorphic mesoproterozoic gneisses and migmatites of upper amphibolite facies from late Neoproterzoic-early Paleozoic times. These rocks are intruded by Neoproterzoic granitoids (Fig. 1) (Muhongo and Lenoir, 1994; Jacobs et al., 1998; Kröner, 2001). East Antarctica is continuing into the Mozambique belt in the north. The Mozambique belt in the Nampula Complex consists of Mesoproterozoic gneisses and migmatites of upper amphibolite facies (Pinna et al., 1993). The sequence of Neoproterozoic-Cambrian amphibolite-facies metamorphism and overlying sedimentary rocks in the Nampula Complex is 520-490 Ma (Bingen et al., 2006a; Bingen et al., 2006b; Bingen et al., 2009). The granulite-facies metamorphism is dated at 615 ± 8 Ma (Kröner et al., 1997). The East Antarctica - and Mozambique belt represents the largest part of EAAO. The northern part is built up of the Arabian-Nubian Shield (ANS) that is composed of Middle-Neoproterzoic island arcs terranes including a number ophiolite assemblage. The ANS reached mid-low metamorphic grade (Stern, 1994). The EAAO is covered by Paleozoic sandstones, which represent the once voluminous molasse shed from the East African–Antarctic orogen (Burke and Kraus, 2000; Avigad et al., 2003).

2.1.2 The Pan-African orogeny

The Pan-African orogeny was a major Neoproterozoic orogenic event, which is associated to the formation of the supercontinents Gondwana about 500 Ma ago (Kröner and Stern, 2005). The Pan-African orogenic belts in Africa are a network encircling the older cratons and are probably due to the closure of several major Neoproterozoic oceans. The name “Pan-African” was first used by Kennedy, (1964). Now it is used to explain tectonic, magmatic, and metamorphic activity of Neoproterozoic to earliest Palaezoic age. It has two types of orogenic or mobile belts and can thus be classified into:

1. Of juvenile origin composed of Neoproterozoic supracrustal and magmatic assemblages; dominated by structural and metamorphic histories that are same to those in Phanerozoic collision and accretion belts (Kröner and Stern, 2005).

2. High-grade metamorphic assemblages revealing middle to lower crustal levels, whose origin environment of formation and structural evolution are more complicated to reconstruct. The protoliths of these assemblages are composed mainly of greatly older Mesoproterozoic to Archaean continental crust that was strongly reworked during the Neoproterozoic, (Kröner and Stern, 2005). The most important orogenies of Pan-African orogeny are Arabian-Nubian Shield, Mozambique belt and Dronning Maud Land.

2.1.2.1 Arabian-Nubian Shield (ANS)

The ANS stretches about 3000 km from north to south and >500 km on either side of the Red Sea, see Fig.1. A large region was uplifted in association with Cenozoic rifting to form the Red Sea, revealing a huge area of typically juvenile Neoproterozoic crust. The Arabian-Nubian Shield (ANS) makes up the northern half of the EAAO and transitions into the Mozambique Belt (Kröner and Stern, 2005). The ANS is dominated by low grade metamorphism and comprises island-arc type rocks and ophiolites with juvenile ages. The final steps in the evolution of the ANS are post-tectonic 'A-type' granites, bimodal volcanics, and molassic sediments. These refer to strong extension happened during orogenic collapse at the end of the Neoproterozoic. Extension related metamorphic and magmatic core complexes are observed in lower numbers in the northern ANS than the southern ANS and the Mozambique Belt (Kröner and Stern, 2005).

2.1.2.2 Mozambique Belt (MB)

The Neoproterozoic Mozambique Belt (MB) is build up of Archaean and Paleoproterozoic rocks. MB characterizes the southern part of the EAAO and is composed mainly of medium to high grade gneisses and voluminous granitoid intrusions. It stretches south from the Arabian-Nubian Shield into southern Ethiopia, Kenya and Somalia via Tanzania to Malawi and Mozambique and also Madagascar belongs to the MB (Fig.1.). Southwards the MB has a continuation into Dronning Maud Land of East Antarctica (Fig.1.). The evolution of the MB resulted from collision between East and West Gondwana, (Kröner and Stern, 2005).

2.1.2.3 Dronning Maud Land (DML), East Antarctica

Dronning Maud Land located east Antarctica. It was continuity of Mozambique Belt to the south. DML comprise different geological events. **The first event**, the basement rocks in Dronning maud land are regionally metamorphosed through the collisional event. The oldest ages of ~1130 Ma match to a time of felsic volcanism which was followed by regional metamorphism (granulite facies metamorphism) and intrusion of granites. The regional metamorphism (high – grade metamorphic event) associated with high numbers of syntectonic granitoids, which intruded between 1090 and 1070 Ma (Jacobs et al., 1998). After the Mesoproterzoic event, there is little evidence for tectonic activity between c. 1050 and 650 Ma, with exclusion of Schirmacher Oasis area, where there is limited evidence for granitoid intrusions at c. 760 Ma (Jacobs et al., 2008). The basement is overlain by late Neoproterozoic -early Paleozoic rocks. **The second event**, the late Neoproterzoic until early Paleozoic collisional history can be divided into three major phases; the First phase is characterized by granulite facies at c. 620Ma (Henjes-Kunst, 2004) associated with anorthosite magmatism at c. 600 Ma (Jacobs et al., 1998). The shallowly inclined structure characterizes this event, and it can be related to the emplacement of thrust sheets (Jacobs et al., 2008). The Second phase is characterized by medium- to high grade metamorphism, between c. 590 and 550 Ma (Jacobs et al., 1998; Jacobs et al., 2003b). During this event tight isoclinal, upright E-W- to ESE-WNW-trending folds were produced. In addition to this, a major shear zone was formed along the southern margin of the mountain range in Orvinfjella. There are also transpressive structures observed throughout the massive that are related to the collisional event (Bauer et al., 2004). This event was cut by extensional shear zone and unreformed intrusion of pegmatites and granite veins with a Cambrian age (Jacobs, Klemd et al. 2003b).

The third event, the late-tectonic phase is associated with extension and magmatism between *c*. 530 and 485 Ma (Engvik and Elvevold, 2004; Jacobs and Thomas, 2004; Jacobs et al., 2003a-a). It comprises gabbros bodies emplaced at *c*. 530–520 Ma, the intrusion of major granite–charnockite plutons at *c*. 510–500 Ma and the introduction of small volumes of sheet-like granites at *c*. 485 Ma. These intrusions are interpreted to be related with the last two events and it is formed from magmatization of high to medium grade metamorphic rocks (Fig. 3.).

Geochronology studies (Frost and Bucher, 1993; Bucher and Frost, 1995) show PT condition of charnockites 900˚c and c.5 bar. Many of the charnockites are retrogressed partially to granite, especially at the contact with the late hydrous granite pockets. The geochemistry of charnockites and associated granitoids is quite heterogeneous, but they are characteristically peraluminous to metaluminous and subalkaline with a tendency into alkaline A-type granite compositions. However they are not typical A-type granites since low contents of Ca, Rb, Nb and Ga are observed and based on (Eby, 1992), they classify as A2-type granitoids, which are related to extensional geodynamic regimes. These granitoids form a voluminous and extensive magmatic suite, covering an area of least 15000 km² in Dronning Maud Land, East Antarctica (Jacobs et al., 1998). All these events summarizing at (Fig. 4)

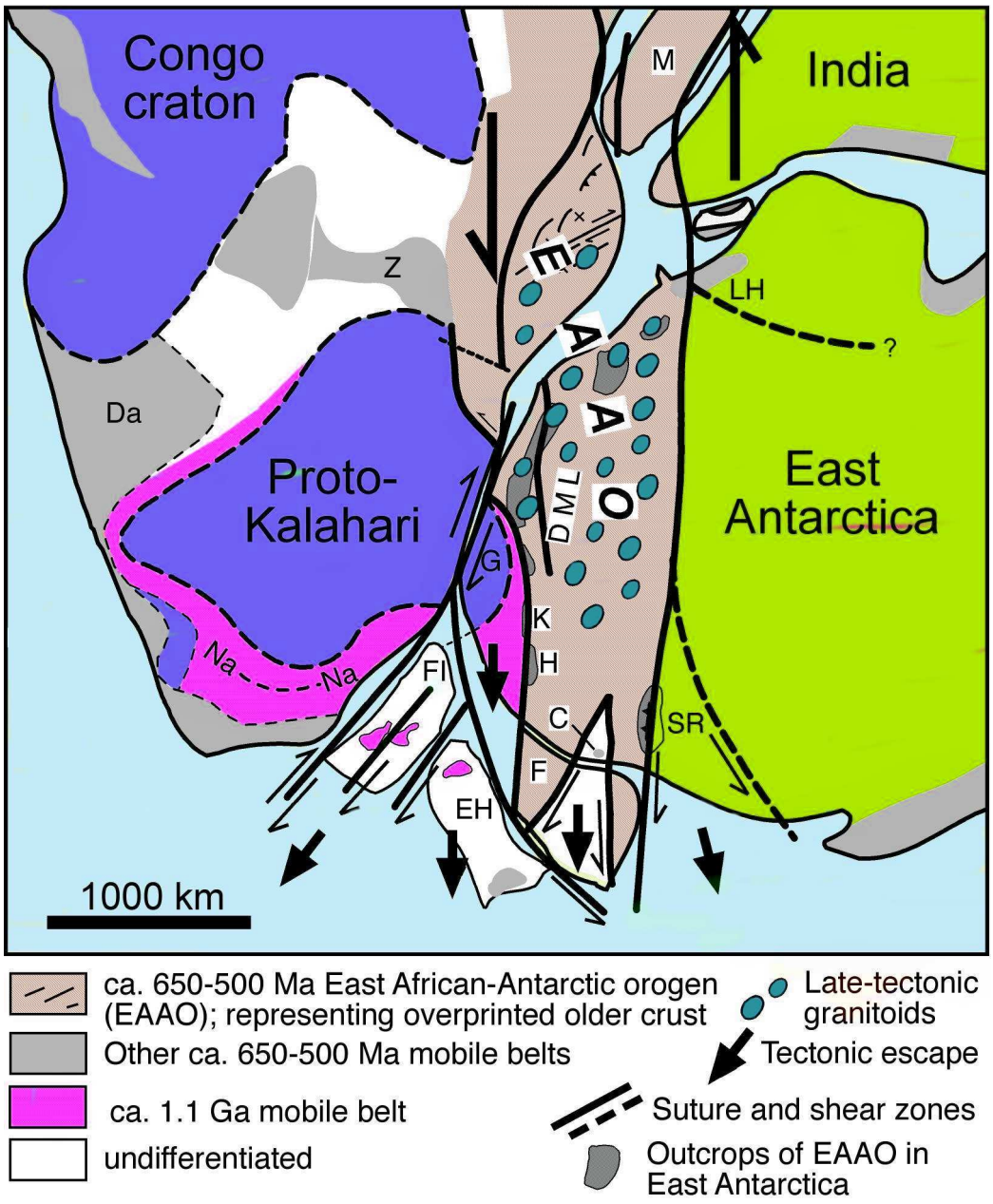

Fig. 3: Escape tectonics model for the southern termination of the East African–Antarctic orogen (EAAO). C—Coats Land; DML—Dronning Maud Land; EF—European fragments; EH—Ellsworth-Haag; F—Filchner block; FI—Falkland Islands; G—Grunehogna; H—Heimefrontfjella; K—Kirwanveggen; Na-Na—Namaqua-Natal; SR—Shackleton Range; ANS—Arabian-Nubian shield; Da—Damarabelt; LH—Lu¨tzow-Holm Bay; M—Madagascar; Z—Zambesi belt after Jacobs and Thomas (2004)

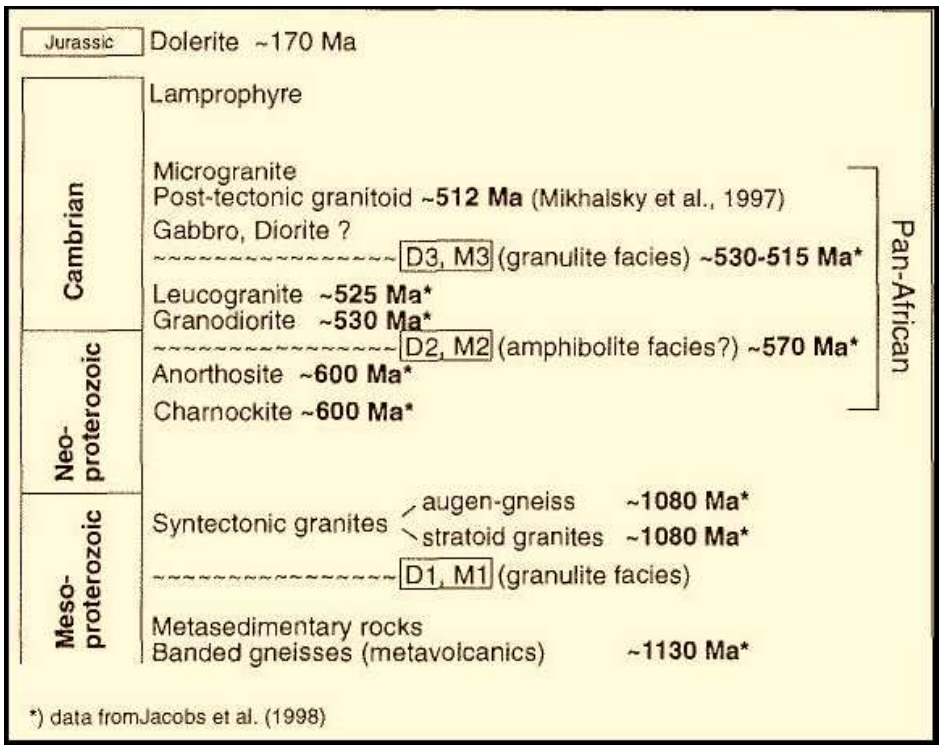

Fig. 4: Evolution of Magmatic and metamorphic basement in CDML as indicated by U-Pb SHRIMP zircon analyses (modified from Jacobs et al., 1998), also publish in (Meier, 1999)

2.3 Tectonic model

There are currently four contrasting tectonic models which can explain the existence of the observed granitoid suite in the southern EAAO (Klimov et al., 1964) that will be presented briefly in the following text.

2.3.1 Thrust faulting model into the north of the Lurio belt

An early French-Mozambiquan study summarized the northern Mozambique orogen related to thrust faulting into the north of the Lurio belt (Pinna et al., 1993), where these authors interpreted the thrust pile that was overthrusted SE along Lurio belt over the Nampula Province as the remains of major latest Mesoproterzoic-early Neoproterzoic (1100-950 Ma). In this model the various rocks late Neoproterzoic and early Paleozoic ages would be expected, but recent work shows that the Lurio Belt has Palaeozoic metamorphic ages. This model is therefore no longer defensible.

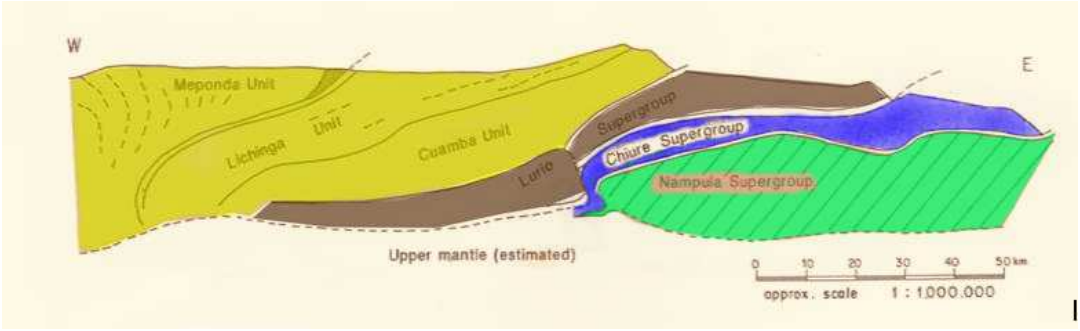

Fig. 5: Thrust model result of Mesoproterozoic collision with flat-lying suture and southwards nappe transport modify from Ueda (2011) after (Pinna et al., 1993).

2.3.2 Overthrusting model SE along the Lurio Belt

The second tectonic model is similar to the one described before but operated at different times resulting in a different age frame. Above the Nampula Complex to the south granulite-facies rocks were overthrust to the SE along the Lurio Belt between c.620 and 550 Ma. The late granitoid magmatism could also be explained by crustal thickening through a SE-directed thrusting of nappes from the combined Damara-Zambesi mobile belt towards Dronning Maud Land (Grantham et al., 2008). Thrust faulting transported the granulite facies rocks from deeper level into upper levels. This model hampers to

explain the Klippen complex in Mozambique, which overlies the Nampula complex. In addition, typical crustal granitoid melts would be expected and not the observed A2-type compositional range for the Pan-African granitoids as described above. At last, the shearing along the Lurio Belt is evidenced at 530-500 Ma (Bingen et al., 2006a; Bingen et al., 2006b), which means the movement is younger than 620-550 Ma. This suggestion is more reasonable since PT condition for retrogression has lower pressure and temperature.

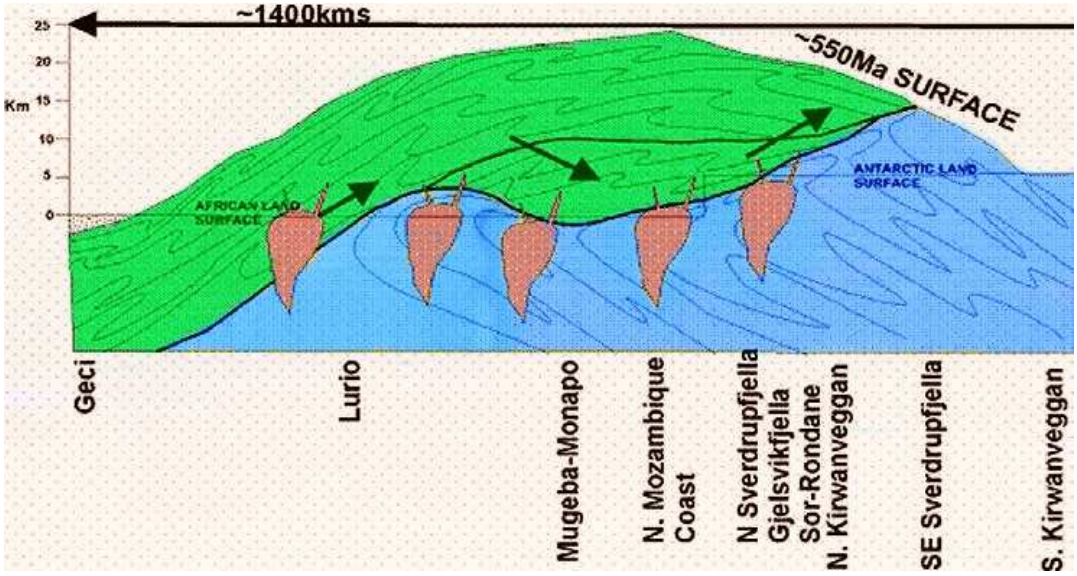

Fig. 6: thrusting model of the Damara-Zambesi mobile belt towards Dronning Maud Land after Grantham et al. (2008).

2.3.3 Thrusting and exhumation model

(3) The third tectonic model includes thrusting and exhumation towards a NW direction to the north of the Lurio Belt. This model explains the granulite-facies rocks at c. 620-550 Ma. This event was followed by the Mesoproterozoic to Neoproterozoic basement terranes at c. 530-490 Ma, northword of the Lurio Belt were as extensional shearing separate between the Nampula Province and the Lurio Belt. The young metamorphic ages which appear in this belt were a result of movement along this shear zone (Norconsult Consortium, 2007).

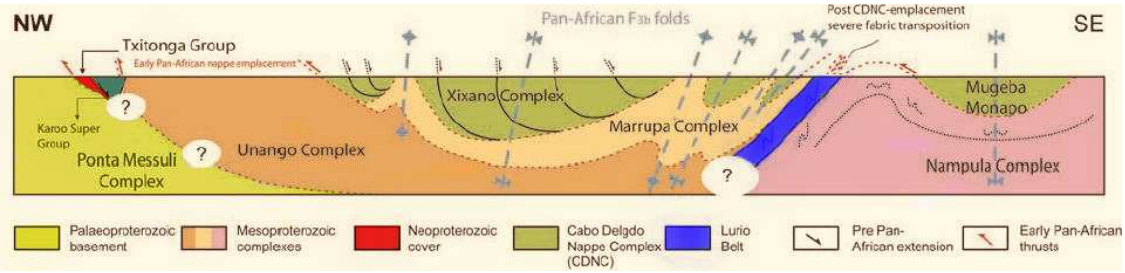

Fig. 7: Model of thrusting and exhumation modify from Norconsult Consortium (2007); also published in (Viola et al., 2008). Blue lines show the axial planes of the large scale folds.

2.3.4 Delamination model

Crustal thickening during orogen built-up may lead to delamination of the orogenic root. This is followed by upwelling of hot asthenosphere under a thinned continental crust. The limited special extend of the granitoid could be explained by a partial delamination, restricted to the area south of the Lurio belt, (Jacobs et al., 2008).

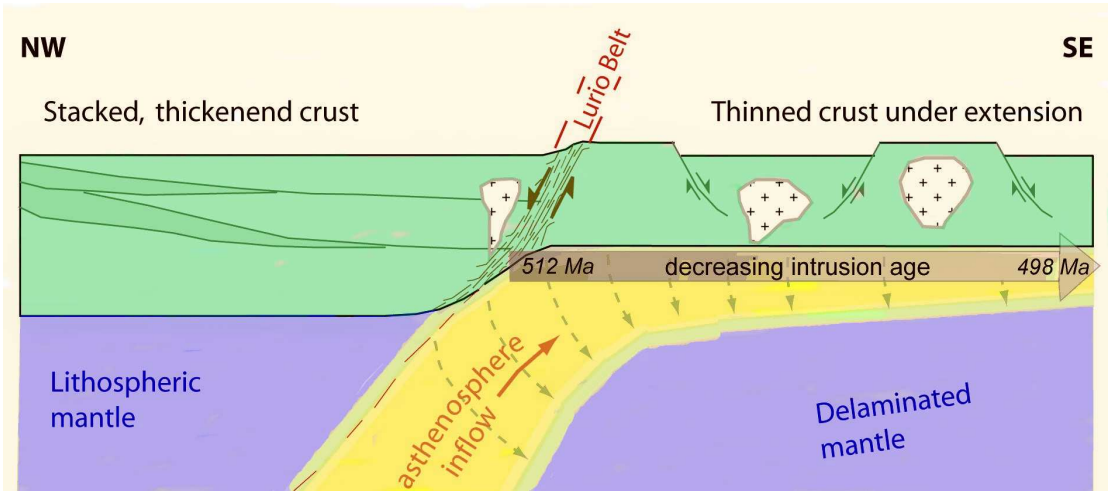

Fig. 8: Delamination model of the area south of the Lurio belt, from northern Mozambique towards Dronning Maud Land, modify from Ueda (2011). It explains removal of lithospheric mantle from underneath the Nampula Complex and the subsequent formation of granitoids.

3. Methodology

3.1 Sample preparation

Samples (JJ1684, JJ1756, JJ1759, JJ1772, JJ1821, JJ1825, and JJ1940) were collected for the U-Pb zircon analysis from different areas in central Dronning Maud Land (cDML), E-Antarctica during the GEOMAUD expedition 1995/1996. Two samples (JJ1684 and JJ1772) are from Holtedahlfjella, samples JJ1756 and JJ1759 are from Shcherbakova/Småskeidrista, and samples JJ1821 and JJ1825 are from the Zwiesel area (Fig.2). I was provided with zircon mineral separates that were prepared with standard procedures (crushing, Wilfley shaking table, magnetic separation, and heavy liquids).

3.2 Preparation of sample mounts

The first step in the sample preparation was to pick single zircon grains. The largest grains (between 90 and 450 µm in length) were selected for analysis to provide enough surface for laser ablation sampling. The grains were attached to a double-sided tape on a glass plate inside a plastic ring that was subsequently filled with epoxy resin. The epoxy resin was prepared by stirring hardener to resin at a ratio of 1:5. It was then heated to remove air bubbles trapped in the resin. The epoxy resin with embedded samples was then dried in an oven at 30 °C for ca. 24 hours. The glass plate was then detached and the relics of the tape were removed by ethanol.

3.3 Grinding

First the mounts were ground by hand in a mixture of water and 800 mesh alumina powder, followed by 1000 and 1200 mesh. The grinding continued until all zircons were exposed approximately in the middle of the grains. Between every step of grinding the mounts were cleaned with water in an ultrasonic bath to remove the grinding powder.

3.4 Polishing

This step involved polishing of the sample surface with diamond paste (3 µm). Then the alumina powder (0.05 µm) was used. Between all polishing steps the mounts were cleaned with water in an ultrasonic bath; then the mounts were dried at room temperature.

3.5 Microscope images

Microscope images were taken for all grains in the mount. The images were used as a map during the analysis.

3.6 Cathodoluminescence (CL) images

Cathodoluminescence images were used to reveal the internal structure of zircon grains to choose the best grains for analysis, including suitable areas for analysis. First the mounts were covered by the thin carbon coating, and using a scanning electron microscope (ZEISS SUPRA 55 VP) equipped with a CL-detector at the University of Bergen to obtain the CL images. Two to three grains were taken in one image. Before analysis the carbon coating was removed from the mount surface by polishing with diamond paste (0.5 μm) for a few seconds. Post-analysis images were obtained in order to check the analyzed areas.

3.7 Zircon dating using LA ICP-MS method

First the mounts were cleaned with ethanol then dried and kept in containers. In the ICP-MS lab, the mounts were cleaned by nitric acid to remove any potential surface Pb contamination. This was done by putting every mount in a small beaker which was filled with 5% HNO_3 acid. Then the beaker was put in an ultrasonic bath for several minutes and the mount was subsequently cleaned with deionized water (18.2 MΩ). Finally the mounts were dried in a stream of air. Then the mounts were ready for analysis.

All three samples were analyzed in the ICP-MS laboratory at Bergen University during 21st and 22nd of March 2011 followed the technique described in (Kosler et al., 2002). A Thermo-Finnigan Element 2 sector ICP-MS coupled to a 193 Excimer Resonetics laser (RESOlution M50) was used to measure Pb/U element ratios and Pb isotopic composition in zircons. The sample introduction system of ICP-MS was modified to enable simultaneous nebulisation of trace solution and laser ablated material of the solid sample (Horn et al., 2000). Tl ($^{205}Tl/^{203}Tl$ = 2.3871 - (Dunstan et al., 1980), ^{209}Bi and enriched ^{233}U and ^{237}Np (>99%) were used in the tracer solution, which was aspirated to the plasma in an argon - helium carrier gas mixture through an Apex desolvation nebuliser (Elemental Scientific) and a T-piece tube attached to the back end of the plasma torch. A

helium gas line, carrying the sample from the laser cell to the plasma, was also attached to the T-piece tube.

The laser was set up to produce a repetition rate of 5 Hz. The laser beam was imaged on the surface of the sample placed in the ablation cell, which was mounted on a computer-driven motorised stage of a microscope. During ablation the stage was moved beneath the stationary laser beam to produce a linear raster (c. 50-100×19 µm) in the sample, (c. 50-100×26 µm) in zircon reference material 91500, (c. 50-100×26 µm) in zircon reference material sample GJ-1 and (c. 50-100×19 µm) zircon reference material Plešovice. Typical acquisitions consisted of a 35 second measurement of analytes in the gas blank and aspirated solution, particularly ^{203}Tl - ^{205}Tl - ^{209}Bi -^{233}U - ^{237}Np, followed by measurement of U and Pb signals from zircon, along with the continuous signal from the aspirated solution, for another 150 seconds. The data were acquired in time resolved - peak jumping - pulse counting mode with 1 point measured per peak for masses 202 (flyback), 203 and 205 (Tl), 206 and 207 (Pb), 209 (Bi), 233 (U), 237 (Np), 238 (U), 249 (233U oxide), 253 (237Np oxide) and 254 (238U oxide). Raw data were corrected for dead time of the electron multiplier and processed off line in a spreadsheet-based program (Lamdate - (Kosler et al., 2002)) and plotted on concordia diagrams using Isoplot (Ludwig, 1999). Data reduction included correction for gas blank, laser-induced elemental fractionation of Pb and U and instrument mass bias. Minor formation of oxides of U and Np was corrected for by adding signal intensities at masses 249, 253 and 254 to the intensities at masses 233, 237 and 238, respectively. Details of data reduction and corrections are described in (Kosler et al., 2002) and (Kosler and Sylvester, 2003). Zircon reference material 91500 (1065 Ma - (Wiedenbeck et al., 1995) used to adjust the composition of the tracer solution. Zircon reference samples GJ-1 (Jackson et al., 2004) and Plešovice (Sláma et al., 2008) were periodically analysed during this study for study for quality control and they yielded concordia ages of 598 ±18Ma and 334 ±6 Ma, respectively.

4. Results

The six samples (JJ1684, JJ1756, JJ1759, JJ1772, JJ1821, and JJ1825) were selected from different areas in center Dronning Maud Land, East Antarctic (Fig. 2) for U-Pb zircon age determination with LA-ICP-MS. The analyses were performed at the University of Bergen during February 2011. Results of the specific samples will be presented throughout the following, from younger to older ages.

4. 1 Sample JJ1684

This sample is classified as biotite-hornblende granite from the Holtedahlfjella area. It contains quartz, two types of feldspars (alkali feldspar and plagioclase), biotite, hornblende and an accessory minerals including zircon. Further, coarse grained perthitic textures with crystal sizes larger than 1 mm are observed (Fig. 9).

1.

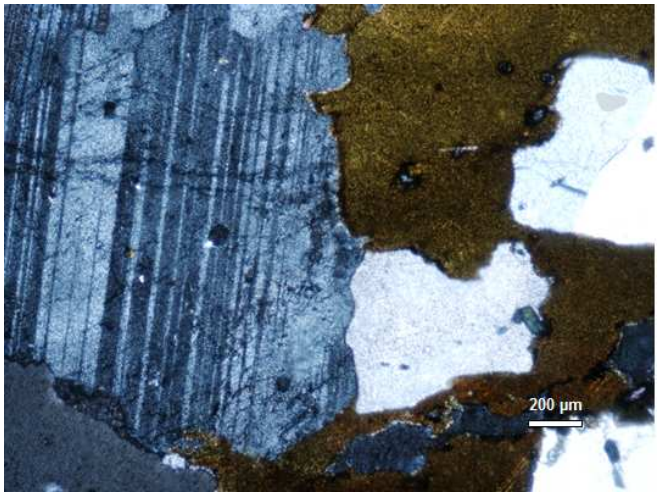

2.

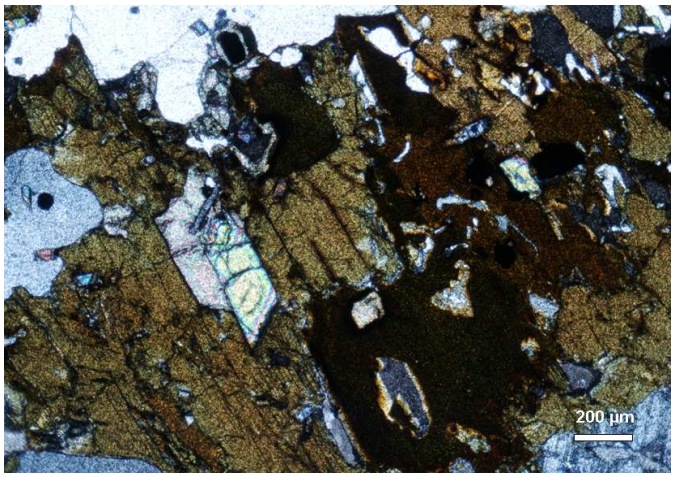

3.

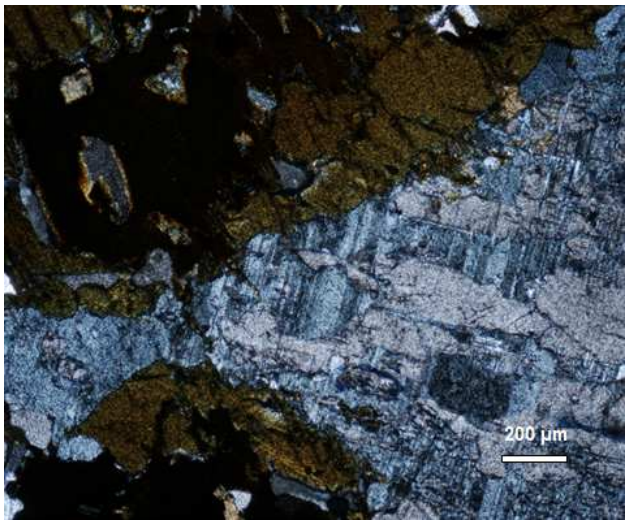

Fig. 9: Photomicrographs of sample JJ1684 (biotite-hornblende granite). (1.) The sample displays brown flaky biotite grains. It shows anhedral crystals of quartz, which have undulose extinction. The euhedral crystals of plagioclase show typical microtwinning. (2.) Greenish brown hornblende grains, which show two sets of cleavage with angle of 124º. The other accessory minerals observed are zircons (high interference color) occurring as inclusion in hornblende. (3.) This photomicrograph shows mesoperthitic texture, which is an intergrowth of two feldspars that

caused by the high temperatures of a K-feldspar-bearing melt absorbing borders of some plagioclase crystals.

This sample consists of yellowish brown to brownish elongated zircons with many inclusions. The CL imaging shows larger zircon grains between 250 and 450 µm in length. The CL imaging reveals a variety in U-content between a core and rim record as oscillatory zoning within most grains.

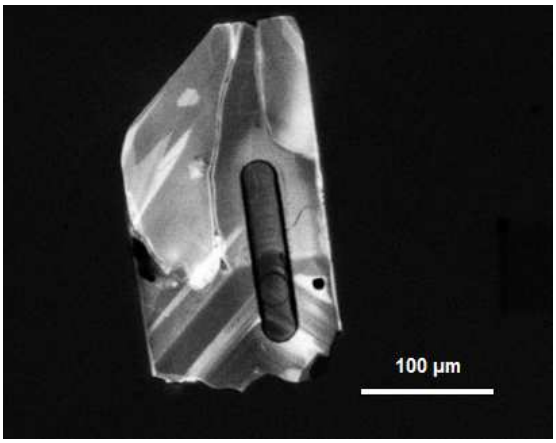

Fig. 10: Post-analysis cathodoluminescence image of a typical elongated zircon from Holtedahlfjella (analyses number 1 (Table. 3), sample JJ1684) with internal zoning. In addition, the laser line of the LA-ICP-MS analysis can be seen.

A total number of 19 zircon grains from JJ1684 were analyzed by laser ablation ICP-MS. Sixteen analyses were accepted and 3 results were rejected due to large uncertainty of calculated age $^{207}Pb/^{235}U$ (70.7, 63.4 and 66). The resulting 16 analysis gave a concordia age of 486 ± 7 Ma, and a probability (of concordance) was 0.17, and a MSWD (of concordance) was 1.9.

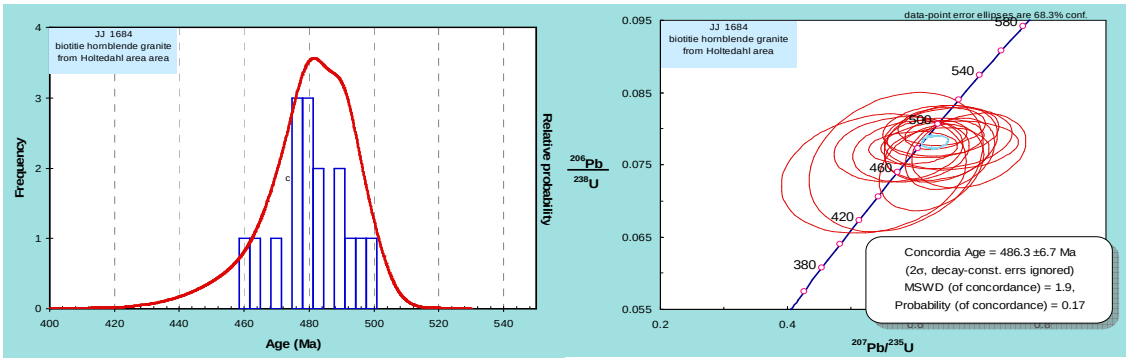

Fig. 11: The left side shows probability density distribution and histograms of detrital zircon $^{206}Pb/^{238}U$ ages from the sample JJ1684. The age represents time interval from 458 Ma to 500 Ma. The right side shows concordia plot diagram of $^{206}Pb/^{238}U$ vs $^{207}Pb/^{235}U$ give a concordia age of 486.3 ± 6.7 Ma, and a probability (of concordance) was 0.17, and a MSWD (of concordance) was 1.9.

4.2 Sample JJ1825

This sample is a synite from the Zwiesel area. It is coarse grained with crystal sizes of larger than 5 mm in diameter. It has a granophyric texture. The sample consists of small amounts of quartz, two types of feldspar (orthoclase and plagioclase), biotite, and biotitic symplectite.

1.

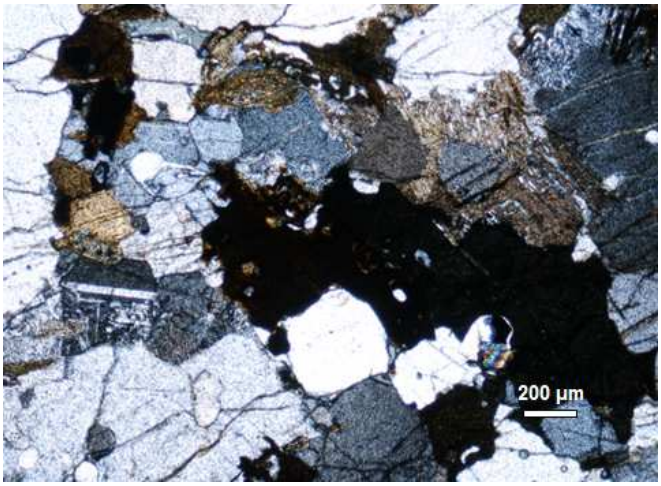

2.

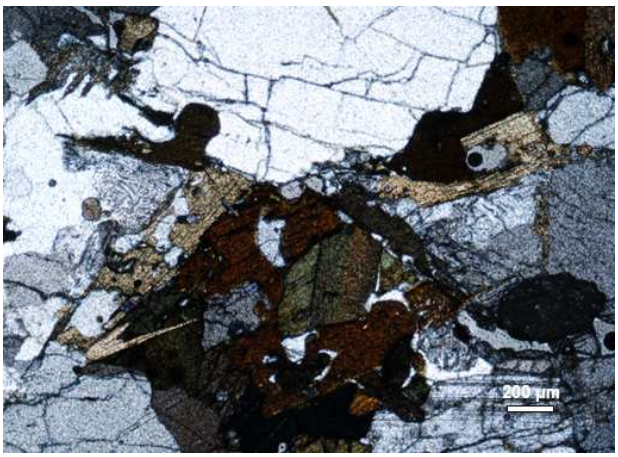

3.

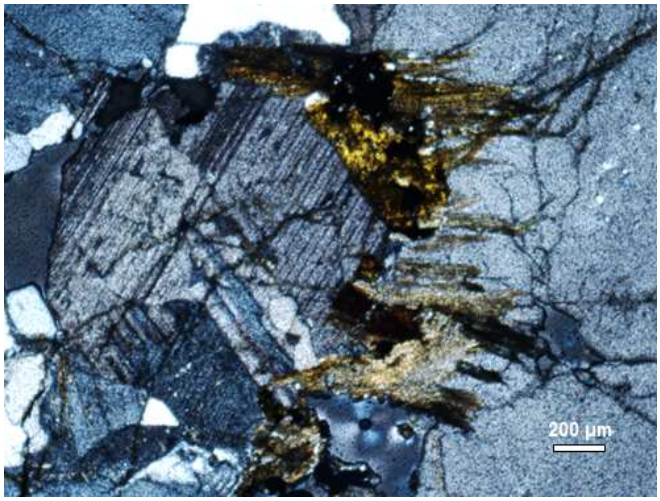

Fig. 12: Photomicrographs of sample JJ 1825 (syenite) (1.) Sample viewed under cross polar light shows hornblende (dark green) and flaky biotite minerals with pale brown to dark brown color. The difference colors of biotite results from strong pleochroism. Also it presents a different kind of altered biotite called biotitic symplectite. The breakdown of unstable biotite is probably the result of rapid cooling. The picture shows anhedral quartz grains, and repeated twinning of plagioclase (in the centre). Also, it presents a granophye texture, which is an

intergrowth between quartz and plagioclase and orthoclase (in the upper part of picture). (2.) This picture shows a graphic texture with inclusions of quartz in the biotite). In the lower right corner a small crystal can be seen that looks like kyanite, which is characerised by a high interference color. 3.) Here a yellow elongated crystal is observed that is assumed to be staurolite. In addition, biotitic symplectite is visible. The big euhedral crystal of microcline shows cross hatch twinning.

This sample contains large zircon grains between 250 µm and 450 µm in length as identified from CL imaging. This sample consists of clear colorless to pale brown elongated zircons with many inclusions. From cathodoluminescence images the zoning of elongated zircon is typical for zircon of igneous origin. Their similarity in size, morphology and internal zoning is interpreted to result from a relatively uniform igneous provenance.

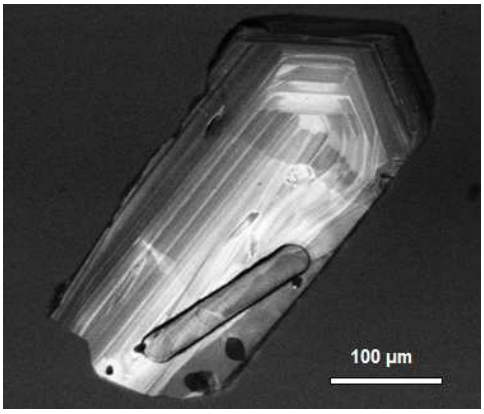

Fig. 13: Post-analysis cathodoluminescence images of selected zircons from Zwiesel area (analyses number 11 (Table.4), sample JJ1825). Elongated zircon has internal zoning.

A total number of 20 zircon grains from JJ1825 were analyzed by laser ablation ICP-MS. Sixteen analyses were accepted and 4 results were rejected due to large errors, one of them was rejected because it has the lower error about (0.0009), so the calculated age for this result is only 129.1 Ma. Three results were rejected due to having large uncertainty of calculated age $^{207}Pb/^{235}U$ (158.8, 72.1 and 60). The calculated concordia age gives 493 ± 5 Ma with a probability (of concordance) of 0.036, and a MSWD (of concordance) of 4.4.

Most of the twenty analyses occur in the light rim, which is clearly in the cathodoluminescence image above (Fig.16), covering the time interval between 478 Ma to 504 Ma.

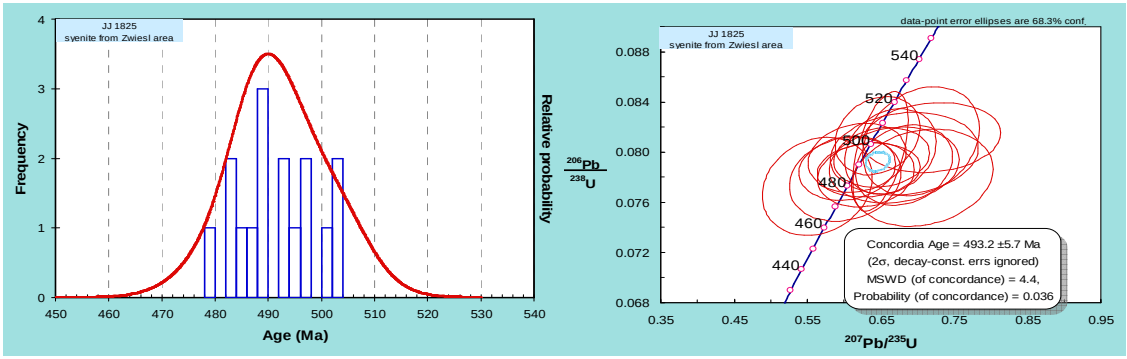

Fig. 14: The left side shows probability density distribution and histograms of detrital zircon ages from the sample JJ1825. The age represents time interval from 478Ma to 504Ma. The right side shows concordia plot diagram of $^{206}Pb/^{238}U$ vs. $^{207}Pb/^{235}U$ give a concordia age of 493 ± 5 Ma with a probability (of concordance) of 0.036, and a MSWD (of concordance) of 4.4.

4.3 Sample JJ1821

This sample is a charnockite (two-pyroxene granitoid) from the Zwiesel area. This sample is medium grained with grain sizes between 0.5 to 1 mm. The mineral assemblage is dominated by quartz, plagioclase, K-feldspar (microcline), biotite, hornblende, and zircon. Within thin section myrmekitic and mesoperthitic texture can be observed

1.

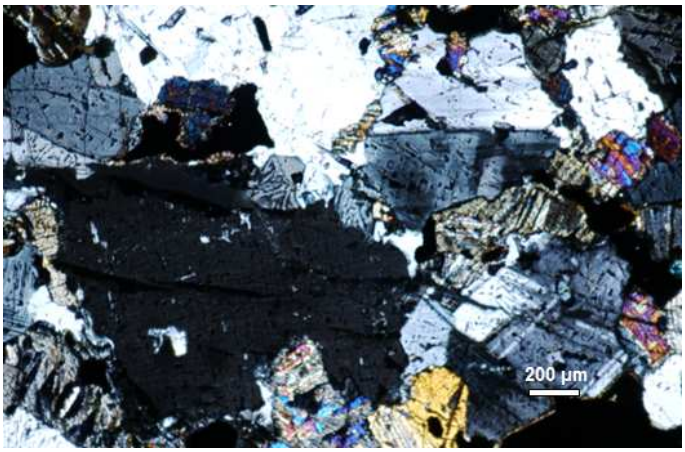

2.

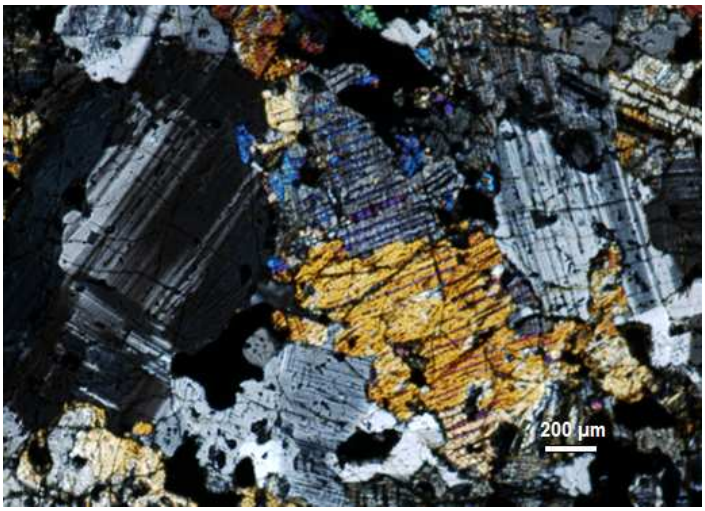

3.

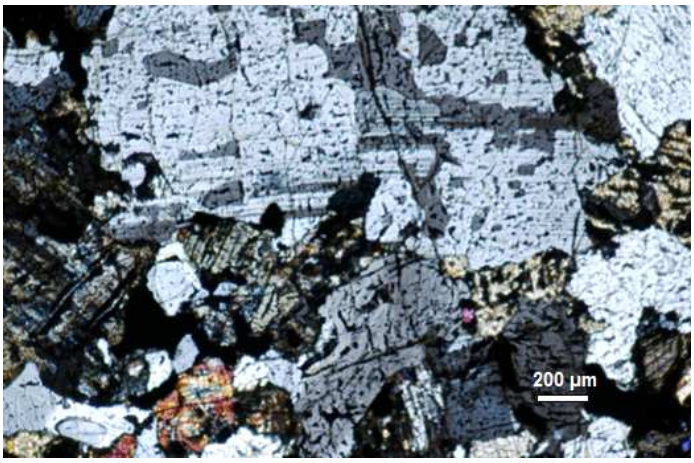

Fig. 15: Photomicrographs of sample JJ1821 (charnockite). (1.) Sample viewed under cross polar light shows second older interference color of pyroxene, anhedral crystals of quartz and subhedral crystals of microcline (crosshatch twinning). (2.) Two types of pyroxene are found, which are orthopyroxene (barrel extinction), and clinopyroxene (oblique extinction). The two types of pyroxene are related to the high P T condition during formation of this rock. Also myrmekite appears as an intergrowth between plagioclase and quartz. (3.) In this picture the mesoperthitic are found, which shows intergrowths of microcline in the joins of plagioclase.

This sample consists of yellowish brown to brownish elongated zircons with many inclusions. From the CL imaging it is seen that all zircon grains range in size between 90 and 300 µm in length. These grains have elongated shapes indicating igneous origin or formation. The grains show dark cores surrounded by lighter rims.

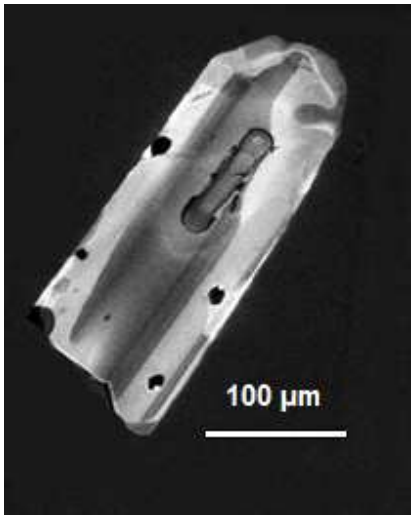

Fig. 16: Post-analysis cathodoluminescence images of a typical zircon grain from Zwiesel area (analyses number 39 (Table. 5), sample JJ1821). The elongated zircon grain is dark in the center and light at the rim.

A total number of 39 zircon grains from JJ1821 were analyzed by laser ablation ICP-MS. Thirty-eight analyses were accepted and only one result was rejected due to a large uncertainty, of calculated age $^{207}Pb/^{235}U$ (101.8). The concordia age provides an age of 513± 4 Ma, and a probability (of concordance) was 0.021, and a MSWD (of concordance) was 5.3. Most of the thirty-eight analyses occur in the light rim that is clearly in the cathodoluminescence image above (Fig.14), covering the interval age between 491 Ma to 530 Ma.

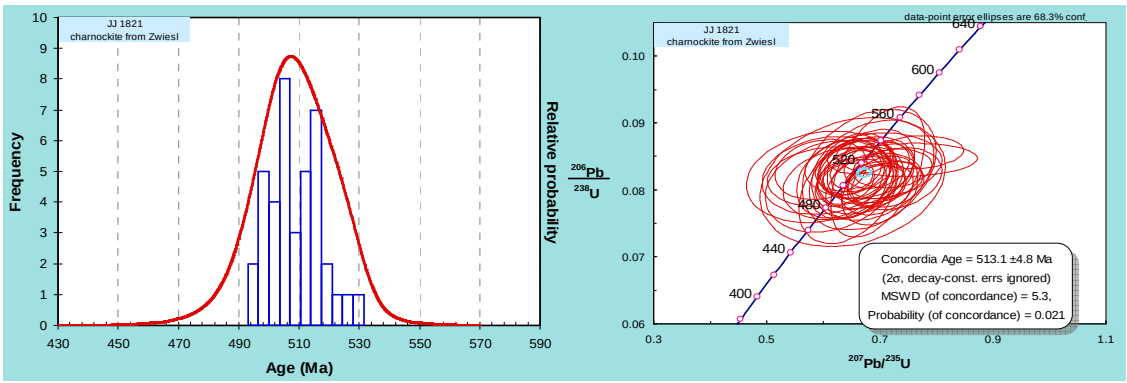

Fig. 17: The left side shows probability density distribution and histograms of detrital zircon ages from sample JJ1821. The age represents time interval from 491 Ma to 530 Ma. The right side shows concordia plot diagram of $^{206}Pb/^{238}U$ vs. $^{207}Pb/^{235}U$ give a concordia age of 513 ± 4 Ma, and a probability (of concordance) was 0.021, and a MSWD (of concordance) was 5.3.

4. 4 Sample JJ1756

This sample is a hornblende gneiss from the Shcherbakova area. From CL imaging, the zircon grains are between 95 and 270 µm in length. This sample consists of colorless brownish rounded zircons without inclusions. Most of the grains have a sub-euhedral to rounded morphology; stubby to rounded zircon grains indicate that zircon grains are similar to themetamorphic zircons. Some grains have zoning whereas others are homogeneous dark in CL image due to high U concentration.

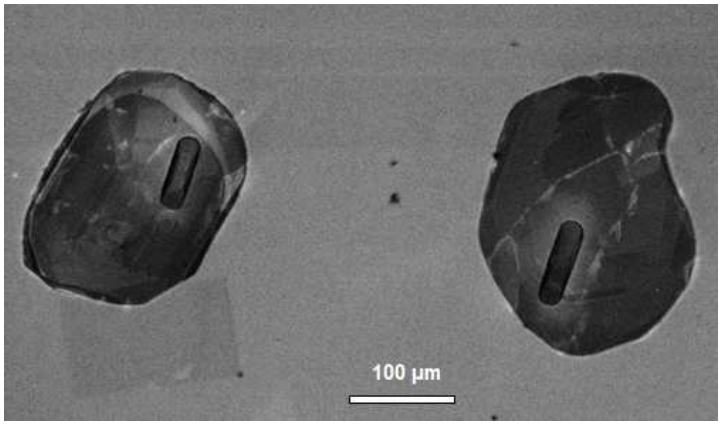

Fig. 18: Post-analysis CL images of selected zircons from Shcherbakova area (analyses numbers 10 and 11 (Table. 6), sample JJ1756). Rounded zircon grains are similar to the metamorphic zircons. Laserlines from LA-ICP-MS can be observed.

A total number of 25 zircon grains from JJ1756 were analyzed by laser ablation ICP-MS. Twenty-two analyses were accepted and 3 results were rejected. One of them was rejected due to large error (0.0102) and two results were rejected due to having large uncertainty of calculated age $^{207}Pb/^{235}U$ (67.4 and 48.4). The 22 analyses give concordia

age of 610 ± 6Ma, and a probability (of concordance) was 0.43, and a MSWD (of concordance) was 0.61. The fifteen analyses were carried out in the core provide ages range from 535 Ma to 610 Ma and five analyses from the surrounding rim give an age from 620 Ma to 680Ma.

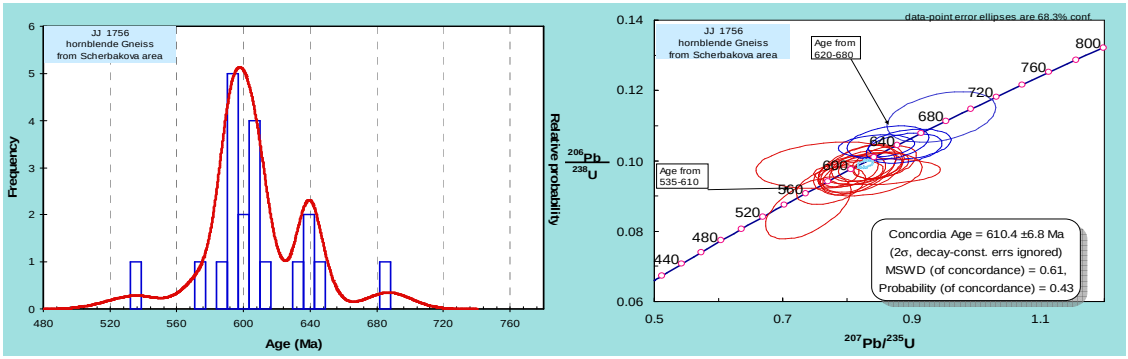

Fig. 19: The left side shows probability density distribution and histograms of detrital zircon ages from the sample JJ1756. The age pattern of this sample shows two different events at around 640 Ma and 680 Ma. The observed age range is from 535 Ma to 610 Ma and age from 620 Ma to 680 Ma. The right side shows concordia plot diagram of $^{206}Pb/^{238}U$ vs. $^{207}Pb/^{235}U$ give a concordia age of 610 ± 6 Ma, and a probability (of concordance) was 0.43, and a MSWD (of concordance) was 0.61.

4. 5 Sample JJ1759

This sample is an amphibolite from the Shcherbakova area. It has large zircon grains ranging from 200 µm to 400 µm in length. This sample consists of clear colorless to pale brown elongated zircons with many inclusions. Cl-images reveal perfect zoning in the elongated zircon. Morphologically all zircons from this sample are interpreted as igneous zircons. These grains are dark in the center and surrounded by light rim pointing to high concentrations of Uranium in the core and low U concentrations in the rim.

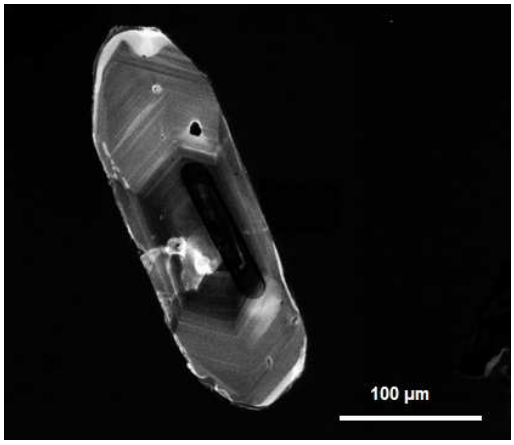

Fig. 20: Post-analysis cathodoluminescence images of a typical zircon from Shcherbakova area (analyses number 11 (Table. 7), sample JJ1759). The elongated zircon grain is dark in the center and shows a surrounding light rim.

A total number of 22 zircon grains from JJ1759 were analyzed by laser ablation ICP-MS. Twenty analyses were accepted and two results were rejected due to large error (0.0108 and 0.0183), and because they have large uncertainty of calculated age $^{207}Pb/^{235}U$ (196.3 and 107). The obtained single grain ages fall into four distinct age groups: Ten analyses was analyzed in the cores present an age of 995-1050 Ma, four analyses taken in the wide rim give an age of (700-820 and 850-920) Ma and the two analyses from the edge of the rim yields an age of 500 Ma and 550 Ma .

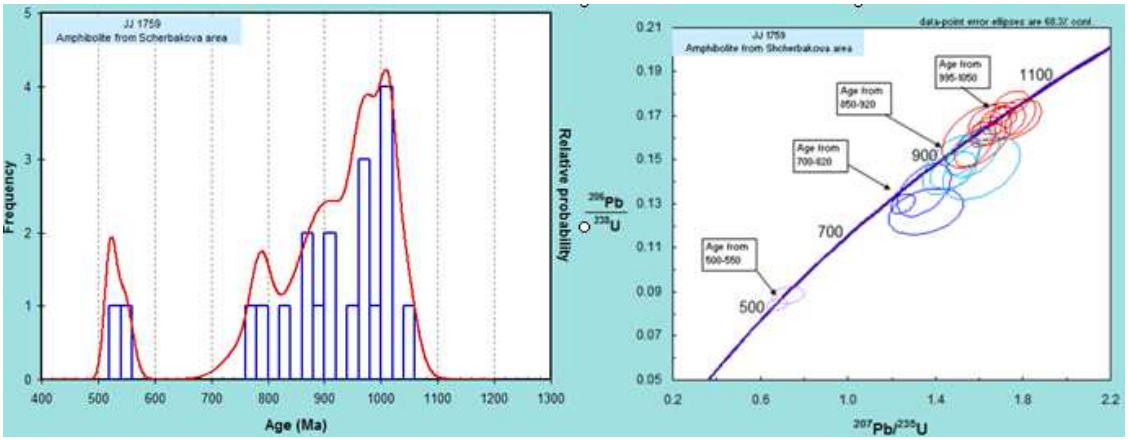

Fig. 21: The left side shows probability density distribution and histograms of detrital zircon ages from the sample JJ1759. The observed age pattern indicates that this sample has suffered at least

three different events: (i) 500 Ma, (ii) 550 Ma, (iii) 700 Ma to 820 Ma and (iv) 850 Ma to 920 Ma (v) 950 Ma to 1050 Ma. These events appear in the cathodoluminescence image above, starting with darkest in the core, lighter rim which surrounded by narrow very light edge (Fig.21). The right side shows concordia plot diagram of $^{206}Pb/^{238}U$ vs. $^{207}Pb/^{235}U$ interpreted from the left diagram.

4. 6 Sample JJ1772

This sample is grey gneiss, which contains only small zoned zircon grains with a size between 95 and 350 µm in length (Fig. 15). This sample consists of clear colorless to pale brown zircons with many inclusions. In cathodoluminescence images the grains appear lighter in the core and darker at the rim, which means that it has low concentrations of Uranium in the centre and high concentrations of Uranium in the rim. This type of zoning generally shows a broadening of oscillatory zones that is characteristic of partial recrystallization. So, the dark rim is interpreted to be due to a new stage of crystallization.

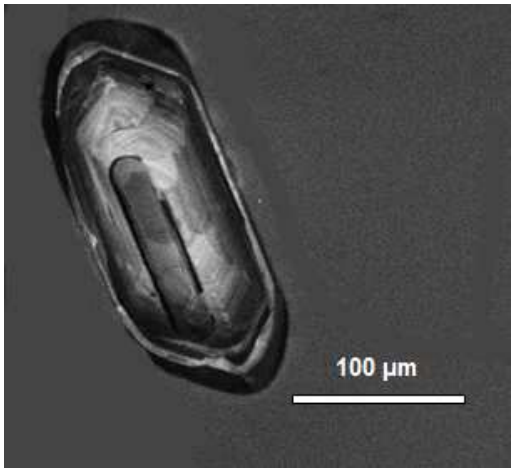

Fig. 22: Post-analysis cathodoluminescence images of a typical zircon grain from the Holtedahlfjella (analyses number 11 (Table. 8), sample JJ1772). The zircon grain shows a slight dark in the core, surrounded by light outer core, followed by a dark and light rim and finally surrounding by a darker edge rim. This grain has several stages of zoning.

A total number of 23 zircon grains from JJ1772 were analyzed by laser ablation ICP-MS. Twenty-one analyses were accepted and 2 results were rejected due to large errors, because of large uncertainty of calculated age $^{207}Pb/^{235}U$ (121.3 and 117.1). The concordia age falls into five different age groups: five analyses provide an age of 1050-1100 Ma, six analyses yield an age of 910-1000 Ma, two analyses give an age of 870-900 Ma, seven analyses of detrital zircon provide age of 750-850 Ma and only one analysis present age of 610 Ma. These difference groups appear clearly in the cathodoluminescence image above (Fig.23) start with the light core surrounding with dark, light rim and finish with the dark rim. The probability (of concordance) was 0.005 and a MSWD (of concordance) was 7.8.

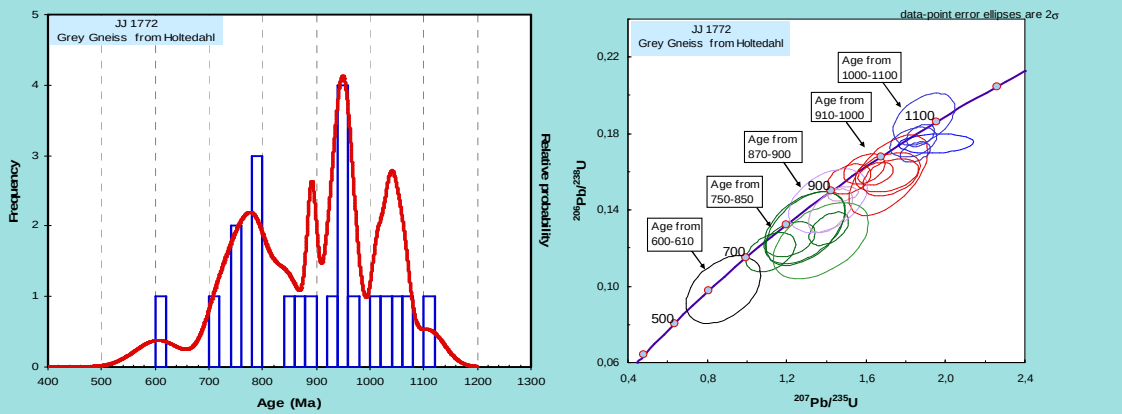

Fig. 23: The left side shows probability density distribution and histograms of detrital zircon ages from the sample JJ1772. The age pattern of this sample indicates four different events with ages of 610 Ma, 750-850 Ma, 870- 900 Ma, 910-1000 Ma and 1050-1100 Ma. The right side shows concordia plot diagram of $^{206}Pb/^{238}U$ vs. $^{207}Pb/^{235}U$ interpreted from the left diagram

Table 1: show the summary of the results of this study in the central Dronning Maud Land

Sample	Rodinia 1, Age (Ma)	Rodinia 2, Age (Ma)	Rifting 1, Age (Ma)	Rifting 2, Age (Ma)	Rifting 3, Age (Ma)	Gondwana 1, Age (Ma)	Gondwana 2, Age (Ma)
JJ1684							458-500
JJ1825							478-504
JJ11821							491-530
JJ1756					620-680	535-610	
JJ1759		950-1050	850-920	700-820		550	500
JJ1772	1100-1050	910-1000	870-900	750-820		600-610	

5. Interpretation

The present study further constraints the occurrence and distribution of gneisses and granitoids in central Dronning Maud Land. The late-tectonic granitoid intrusions are interpreted to reflect the timing of the metamorphism during final Gondwana collision.

5.1 Granitoids from central Dronning Maud Land

The granitoids can be discriminated into two groups: (i) intrusions related to the formation of Gondwana and (ii) Post intrusions during Pan-African II.

5.1.1 Collapse and extension in Dronning Maud Land

Compared to previous studies mentioned in Table 2, the general results of this study shows strong similarities to the known main magmatic/metamorphic episodes from Dronning Maud Land. Most of these results further confirmed the occurrence of granitoid intrusions in central Dronning Maud Land during 450 Ma to 530 Ma related to the Pan-African orogeny (late Gondwana assembly 2). The Pan-African II event (Fig. 29) occurred between ca. 520 Ma to 480 Ma (Cambrian events), (Jacobs et al., 2003a) and is interpreted as the time of orogenic collapse, which was followed by large-scale extension that started at ca. 530 Ma. As the result of this collapse and extension, voluminous large number of small intrusions of post-tectonic mostly A2-type granitoids were placed into the crust now exposed in central Dronning Maud Land (Jacobs et al., 2008).

The Concordia age of sample **JJ1684** is 486 ± 6 Ma that can also be understood as magmatic intrusion occurred during final Gondwana collision.

This result is almost similar to the age of a post-tectonic granite sheet with 487 ± 4 Ma, which was investigated by Jacobs et al., (2003a (Timing)), from the Gygra in Gjelsvik-Fjella (Fig. 25). This granite was formed by fluidated charnokites, using U-Pb SHRIMP method (Table. 3). Additionally, Engvik and Elvevold, (2006) describe an U-Pb titanite

age of 486 ± 6 Ma for a charnokite from the Trollslottet in Filchnerfjella (Fig. 25) that they interpret as time of fluidisation (Table. 3).

Thus the result for sample **JJ1684** is interpreted to indicate formation during the Pan-African II event.

The concordia yields an age of 493 ± 5 Ma was obtained from the sample **JJ1825**. This data is somewhat similar to the concordia ages of the gabbro (527 ± 6 and 521 ± 6 Ma) was obtained from the Zwiesel area in Wohlthatmassiv (Fig. 25), using U-Pb SHRIMP method (Table 2), (Jacobs et al., 2003b). This result is agrees nicely with the date of a Post-tectonic granite (age of 499 ± 4 Ma) from the Gjeruldsenhøgda in Orvinfjella (Fig. 25), which was found by Jacobs et al., (2008) (Table 2), (Using U-Pb SHRIMP method). This age of 494 ± 5 Ma can also be interpreted as magmatic intrusion during final Gondwana collision. It corresponds with the Pan-African II event which covers the time interval between 520 Ma and 480 Ma (Fig. 29).

The evidence for extension and collapse was stated on the previous study (Jacobs et al., 2008). The occurrence of the high grade granulite-facies root which also, indicates that exhumation of the deepest crustal levels occurred during the extension and collapse. Persistently, the results of this study showed that timing of high-temperature metamorphism can be recognized. This timing is recognized by two kinds of pyroxenes in the charnockite from the Zwiesel area which have age of 513 ± 5, which was revealed from the data of sample **JJ1821**.

Further more, similar age were found in previous studies (Table 2), (Jacobs et al., 1998). This author recognizes as age for a high- metamorphic overprint ca. 522 ±10 Ma in the felsic gneiss from the Dallmannberge in Orvinfjella (Fig. 25), (using U-Pb SHRIMP method). In addition, the age of ca. 521 ± 3 Ma resulted from charnockitised orthogneiss from the Hochlinfjellet in Mühlig-Hofmanngebirge east of central Dronning Maud Land (Fig. 25) was investigated using U-Pb SHRIMP, (Jacobs et al., 2003a (Timing)) (Table 2).

The present result of sample **JJ1821** shows a similar age to the intruded gabbro (527 ± 6 and 521 ± 6 Ma) derived from Zwiesel area in Wohlthatmassiv (U-Pb SHRIMP (zircon Crystallisation (Table 2)) (Jacobs et al., 2003b).

One result measure age of 500 Ma was obtained from the sample **JJ1759**, This sample is an amphibolite also can be explained as the last stage of the magmatization it was happened during Pan African II.

The high grade metamorphism was interpreted to be associated with the magmatic intrusion during the period of Pan-African II was between 520-480 Ma which, characterized by high grade metamorphism intruded by magmatic intrusions (Jacobs et al., 2008).

The similarities were obtained by comparing the results of the current study during 450-530 Ma and the previous mentioned studies (Table 2) that indicated the reliability of the ages measured. Central Dronning Maud Land was established to be characterized by the metamorphisms event associated with the late-tectonic magmatic intrusion. Moreover the collapse and extension of supercontinent Gondwana during Pan-African II event was followed by late-tectonic magmatic intrusion.

These all the ages were mentioned above is nice good agreement with date of ca. 530-495 Ma found in the Nampula complex. The Nampula complex is characterized by Mesoproterozoic gneisses and granulites that were intruded by relatively large volumes of late-to post-tectonic alkali granitoids of the Murrupula Suite, (Macey et al., 2007; Grantham et al., 2008; Jacobs et al., 2008).

Furthermore, it seems that the tectonic evolution of Nampula complex in northern Mozambique and central Dronning Maud Land, East Antarctica, were similar during the Pan-African II event, which indicates the continuity of Mozambique Belt southwards into East Antarctica in central Dronning Maud Land as proposed example by the previous study of (Jacobs et al., 1998).

5.1.2 continent-continent collision during Gondwana supercontinent assembly

In this study, the age of 550 Ma in one zircon grain that is revealed from the data of sample **JJ1759**, can be interpreted as overgrowth of zircon rim caused by magmatization during the Pan-African I event. There is strong agreement between this age and other similar studies describing the same age pattern (Jacobs et al., 1998; Jacobs et al., 2003a (Timing); Jacobs et al., 2003b; Bisnath et al., 2006; Jacobs et al., 2003a).

The age of 550 Ma, which is identified in this study, from metamorphic rocks in cDML is a typical result of its kind (Jacobs et al., 1998; Jacobs et al., 2003a). This author interpreted it as the timing of metamorphism related to collision and following post-collisional magmatism.

Comparison with a previous study (Table 2), this has shown that the age of ca. 557 ±11 Ma are obtained felsic gneiss from the Dallmannberge in Orvinfjella in the central Dronning Maud Land, and located to the west of it (Fig. 25). The method applied by that study was U-Pb SHRIMP methods (Jacobs et al., 1998). The result from that study was explained as metamorphism event between ca. 590 and 550 Ma which represents the collision phase of East-west Gondwana assemblages (Jacobs et al., 1998; Jacobs et al., 2003b). Furthermore, an age of 559 ± 6 Ma revealed in an intrusive leucosome from the Hochlinfjellet in Mühlig-Hofmanngebirge west of central Dronning Maud Land (Fig. 25) was obtained by Jacobs et al., (2003a (Timing)) using the U-Pb SHRIMP method (Table 2). In addition, an age of 566 ± 42 Ma in a banded gneiss from the von Essenkarvet in Gjelsvik-Fjella was obtained by applying the method of U-Pb SHRIMP (zircon) (Bisnath et al., 2006). This age was represented as zircon overgrowth during magmatization. This was examined by applying U-Pb SHRIMP methods (Table 2), to determine the age of 570 ± 3 Ma for the felsic gneiss in the Conradgebirge in the Orvinfjella west of the central Dronning Maud Land (Fig. 25) (Jacobs et al., 1998). In a leucocratic metavolcanic from Trapezberg in the Sivorg west of the Dronning Maud Land (Fig. 25), age was measured as 555 ± 4 Ma by Jacobs et al., (2003a (Timing)). By using SHRIMP

methods, this age was explained as metamorphic zircon rim during the Gondwana assemblages.

The tectonic evolution of the central Dronning Maud Land is further constrained by the result of the current study and supports earlier interpretations and conclusions from previous studied (Table 2). Central Dronning Maud Land (Fig. 2) illustrated by magmatic and metamorphic overprinted during Pan-African I event. This event correlated with collision of the East-West Gondwana (Fig. 26). Early Pan-African episode (early stages of the Gondwana assembly) started with the granulite facies and the amphibolite facies then followed with granitoids intrusion.

One of the results of zircon grain which, measure the age of 610 Ma that was obtained from the sample **JJ1772** that indicates to occurring is coeval to the Early Pan-African (early Gondwana assembly I).

This metamorphic episode is most probably correlated to the age of 610 ± 7 Ma that was revealed from the data of sample **JJ1756**. This age is typical to the charnockite from the Early Pan-African (early Gondwana assembly 1) from the Petermannketten in Wohlthatmassiv (Fig. 25) reported by Jacobs et al., (1998) using U-Pb SHRIMP method (Table 2); and also likely correlated to the age of 600 ± 12 Ma (Table 2) reported by (Jacobs et al., 1998) from the Grubergebirge anorthosite in Wohlthatmassiv (Fig. 25). The intrusions of anorthosite and charnockite from Wohlthatmassiv was at approximately 605 Ma, then followed by deformation and metamorphism between 580 Ma and 540 Ma ((Jacobs et al., 1998; Board et al., 2005; Jacobs et al., 2003a), (Table 2)).

Furthermore this age is comparable with ages obtained from metapelites Schirmacher Oase (Fig. 25) age of 629 ± 3 Ma and 639 ± 5 Ma was done by Ravikant et al., (2007), using U-PB ID TIMS (monazite) method (Table 2). This age can also be interpreted as representing two different events, namely age from 535 Ma to 610 Ma and age from 620 Ma to 680 Ma. The time range of 535-610 Ma is represented by the formation of the amphibolite facies in the early steps of Gondwana assembly 2. The hornblende gneiss

from the Shcherbakova area is related with partial melting and magmatisation of the granulite facies that was related to the formation of the supercontinent Gondwana during Early Pan-African episode (Fig. 26). This event between c. of 530 Ma to 620 Ma is perhaps a result of the crustal convergence it was attained by high-temperature metamorphism, which was characterized by decompression from moderate to high pressures (Board et al., 2005; Jacobs et al., 2003a) related with collision of East-West Gondwana (Fig. 28). That was followed by magmatic character and was marked by the intrusion of large volumes of post-tectonic granite between 490 Ma and 530Ma (Ohta et al., 1990; Mikhalsky et al., 1997; Jacobs et al., 1998; Roland, 2002; Paulsson and Austrheim, 2003; Jacobs et al., 2003b (New); Jacobs et al., 2003a).

The timing of high pressure metamorphism is constrained to the age between 585-660 Ma (John et al., 2004b) and is interpreted as a pre-collision subduction beneath the Kalahari Craton (John et al., 2004a). In the present study the hornblende gneiss was obtained in **JJ1756** (535-680 Ma) from the Shcherbakova is nice agree with the Kalahari Craton. The interval time of 620-680 Ma obtained from this sample can be explained as pre-collision subduction region.

5.1.2 Data from meta-sediments

So far there is no data from meta-sediments. In contrast with a previous study (Table 2) in DML, the new age was obtained in Dronning Maud Land for the first time. It included the time range of ca. 620-680 Ma which was obtained from sample **JJ1756,** 750-850 Ma and 820-920 Ma which was revealed within the sample **JJ1759** and times interval of 750-850 Ma and 870-900 Ma that was revealed by same **JJ1772**. 'The crystallization ages of basement rocks from central DML fall into two broad age groups between 1130 to 1070 Ma and 600-510 Ma' (Jacobs et al., 1998). This, together with the last evolution of magmatic and metamorphic basement in CDML (Fig.4) is not agreeing with the results obtained in the present study.

The interval time of 620-680 Ma which is located between ca. 600 and 750 Ma, the date of the accumulation took place among the Arabian-Nubian Shield (ANS), (Abdelsalam et

al., 2002; Johnson and Woldehaimanot, 2003). Thus this age may be of some magmatic intrusion within the rifting associated with the opening of the ocean. This was equivalent to the accommodation among the ANS.

The age of 750-850 and 700-820 Ma revealed from the detrital zircon within **JJ1772 and JJ1759**, which are comparable to be the age of some zircon grain formation in another region, and then deposit there in Holtedahlfjella that took place during the collapsibility and extension related with ocean opening. So far this sample faced some stage of deformation due to high grade metamorphism, also the disconcordia age of **JJ1759** (Fig. 21) is also explain that. Furthermore the disconcordia age of **JJ1772** (Fig. 23) is also explain that. Also detrital zircon in (Fig. 24) can be interpreted that.

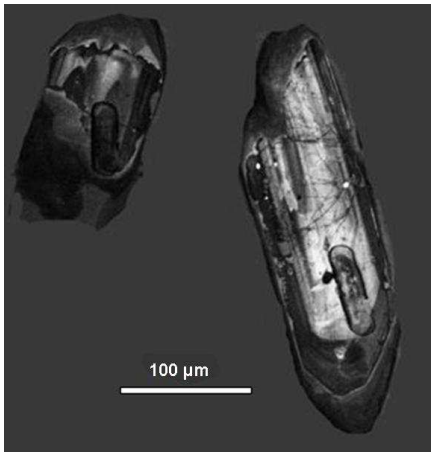

Fig. 24: Post-analysis cathodoluminescence images of a typical zircon grain from the Holtedahlfjella (sample JJ1772). The zircon grain shows a slight dark in the core, surrounded by light outer core, followed by a dark and light rim and ultimately surrounded by a darker edge rim. This grain looks very deformed interpreted detrital zircon.

The time interval 870-900 Ma and 820-920 Ma, can be interpreted as the timing of the metamorphism phase occurred during the collapsed and extension related to the rifting of Rodinia (Fig. 27 & 28).

Finally we can conclude these times range mention above as the several metamorphism phase happened in the central Dronning Maud related to the great rifting associated to the ocean opening, see (Fig. 27 & 28).

These ages are a Known phase of rifting and short-time break-up of Gondwana after Rodinia break-up and before final assembly of Gondwana. It is new that they are occurring with wider areas of central Dronning Maud land. They are known only in the Petermannketten, Grubergebirge and Schirmacher Oasis before.

5.1.3 Old ages and correlation with the Rodinia formation

The age of 950-1050 Ma was revealed from the sample **JJ1759** and the age of 910-1000 Ma and ca. 1050-1100 Ma come from the sample **JJ1772**. These respectively well agree with the Grenvillian metamorphosed felsic volcanic episode interpreted in the literature (Bisnath et al., 2006; Jacobs et al., 1998; Jacobs et al., 2003a (Timing)), (Table 2).

Previously study in the DML was done by (Jacobs et al., 1998), using the U-Pb Shrimp method on zircon, revealed concordant ages of felsic gneiss 1073 ± 9 Ma, 1076 ± 14 Ma and orthogneiss age 1087 ± 28 Ma in the Dallmannberge from Orvinfjella (Fig. 26). They interpreted as corresponding with the magmatic episode responsible for the Rodinia formation (Fig, 27). In the Grenville province felsic metavolcanic episode was occurred in this study area. Furthermore from a grey migmatitic gneiss ages of 1142 ± 21 and 1061 ± 56 Ma (Table 2) were obtained from Festninga in Mühlig-Hofmanngebirge in central Dronning Maud Land, and located to the west of it, see (Fig. 26), which was obtained by detrital zircon SHRIMP, (Jacobs et al., 2003b (New)). These results are not agreement the high grade metamorphism from the Nampula block, which has an age of ca. 1130 to 1100Ma (Macey et al., 2010). But it is slightly agreement with the magmatic phase ages range between 1095-1090 Ma, and medium to high grade metamorphism during interval time 1090-1070 Ma, (Bingen et al., 2009).

Thus the central Dronning Maud land in this study can be responsible with the Grenville province felsic metavolcanic episode.

Table 2: some literature review from Dronning Maud Land

Locality1	Lithology	sample	Date (1200-600 Ma)	Date (600-486 Ma)	Reference
websterite	metapelite	MS 1/23	629±3		(Ravikant et al., 2007)
websterite	metaquartzite	MS 2/23	639±5		(Ravikant et al., 2007)
Grubergebirge	anorthosite	J1955	600±12	555±11	(Jacobs et al., 1998)
Petermannketten	felsic gneiss	J1838	1130±12	~575	(Jacobs et al., 1998)
Petermannketten	charnockite	J1886	608±9	544±15	(Jacobs et al., 1998)
Petermannketten	posttectonic charnockite	J1870		501±7	(Jacobs et al., 2008)
Zwiesel	gabbro	J1818		527±6	(Jacobs et al., 2003b)
Zwiesel	gabbro	J1817		521±6	(Jacobs et al., 2003b)
Zwiesel	charnockite	JJ1821		513±4	Present study
Zwiesel	syenite	JJ1825		493±5	Present study
Gjeruldsenhøgda	granite	J1670		499±4	(Jacobs et al., 2008)
Småskeidrista	qtz-fsp-grt-gneiss	JJ1756	610.4±6.8		Present study
Småskeidrista	amphibolite	JJ1759	~1000		Present study
Dallmannberge	felsic gneiss	J1671	1073±9		(Jacobs et al., 1998)
Dallmannberge	felsic gneiss	J1704	1137±21	522±10	(Jacobs et al., 1998)
Dallmannberge	felsic gneiss	J1795	1076±14	557±11	(Jacobs et al., 1998)
Dallmannberge	orthogneiss	J1797	1087±28		(Jacobs et al., 1998)
Conradgebirge	leucosome	J1745		516±5	(Jacobs et al., 1998)
Conradgebirge	orthogneiss	J1736	1086±20	~570	(Jacobs et al., 1998)
Conradgebirge	metagranodiorite	J1698		530±8	(Jacobs et al., 1998)
Conradgebirge	metaleucogranite	J1695	~1200	527±6	(Jacobs et al., 1998)
Holtedahlfjella	coarse-grained granite	JJ1684		486±6	Present study
Holtedahlfjella	grey migmatitic gneiss	JJ1772	~950		Present study
Trollslottet	charnockite	locality 3		486±6	(Engvik and Elvevold, 2006)

Locality1	Lithology	sample	Date (1200-600 Ma)	Date (600-486 Ma)	Reference
Habermehlgipfel	charnockite	GM733		~540	(Markl and Henjes-Kunst, 2004)
Hochlinfjellet	Charnockitised orthogneiss	1301/2		521±3	(Jacobs et al., 2003a (Timing))
Hochlinfjellet	intrusive leucosome	0801/3		559±6	(Jacobs et al., 2003a (Timing))
Festninga	Hornblende leucosome	1801/1	1088	510±14	(Jacobs et al., 2003a (Timing))
Festninga	grey migmatitic gneiss	1701/2	1142±21	528±10	(Jacobs et al., 2003b (New))
Festninga	grey migmatitic gneiss	1701/3	1061±57	528±11	(Jacobs et al., 2003b (New))
Gygra	Post-tectonic granite sheet	3112/2		487±4	(Jacobs et al., 2003a (Timing))
Risemedet	Late tectonic lamprophyre	2312/2		528±10	(Jacobs et al., 2003a (Timing))
Risemedet	Late tectonic lamprophyre	2312/2		508±7	(Jacobs et al., 2003a (Timing))
Risemedet	migmatitic augen gneiss	2412/4	1096±8		(Jacobs et al., 2003b (New))
Risemedet	augen geniss	1512/1	1123±21/ 1049±19		(Jacobs et al., 2003b (New))
Risemedet	migmatitic augen gneiss	1812/5	1137±14/ 1072±12		(Jacobs et al., 2003b (New))
Stabben	Gabbro	ABA/64	~1100	487±4	(Bisnath et al., 2006)
Stabben	Gabbro	0501/2		483±11	(Jacobs et al., 2003b)
Jutulhogget	migmatite gneiss	ABA/81	1130±19/ 1070	530	(Bisnath et al., 2006)
Jutulhogget	migmatite gneiss (leucosome domain)	WBJS3	1133±15 (core at 1206±19)	526±6	(Bisnath et al., 2006)
Armlenet	sheared felsic gneiss	J3012	1098±25	507±9	(Jacobs et al., 2008)
Armlenet	grey migmatitic gneiss	2712/4	1115±12		Jacobs et al (2003b)
Terningskarvet	grey migmatite gneiss	ABA/21		529 ± 4	(Bisnath et al., 2006)

Locality1	Lithology	sample	Date (1200-600 Ma)	Date (600-486 Ma)	Reference
von Essenkarvet	Augengneiss	ABA/10A	1124±11	417±95	(Bisnath et al., 2006)
von Essenkarvet	aplite dyke	ABA/69		497±5	(Bisnath et al., 2006)
von Essenkarvet	banded gneiss	ABA/32	1120	566±4	(Bisnath et al., 2006)
von Essenkarvet	banded gneiss	ABA/33	1091 ± 17	527±5	(Bisnath et al., 2006)

comment

Locality		Methods	Age	Age	Reference
Schirmacher Oase	Metamorphic	zrc for Amel MSc ICP--MS	1200-950 Ma	570-530 Ma Pan-African I	
Wohlthatmassiv		U-PB ID TIMS (monazite)	640-610 Ma	530-415 Ma Pan-African II	
Orvinfjella	intrusion	U-Pb SHRIMP (zircon)	**NO age**	**NO age**	
Filchnerfjella		U-Pb SHRIMP (zircon)			
Mühlig-Hofmanngebirge		U-Pb Method			
Gjelsvikfjella					

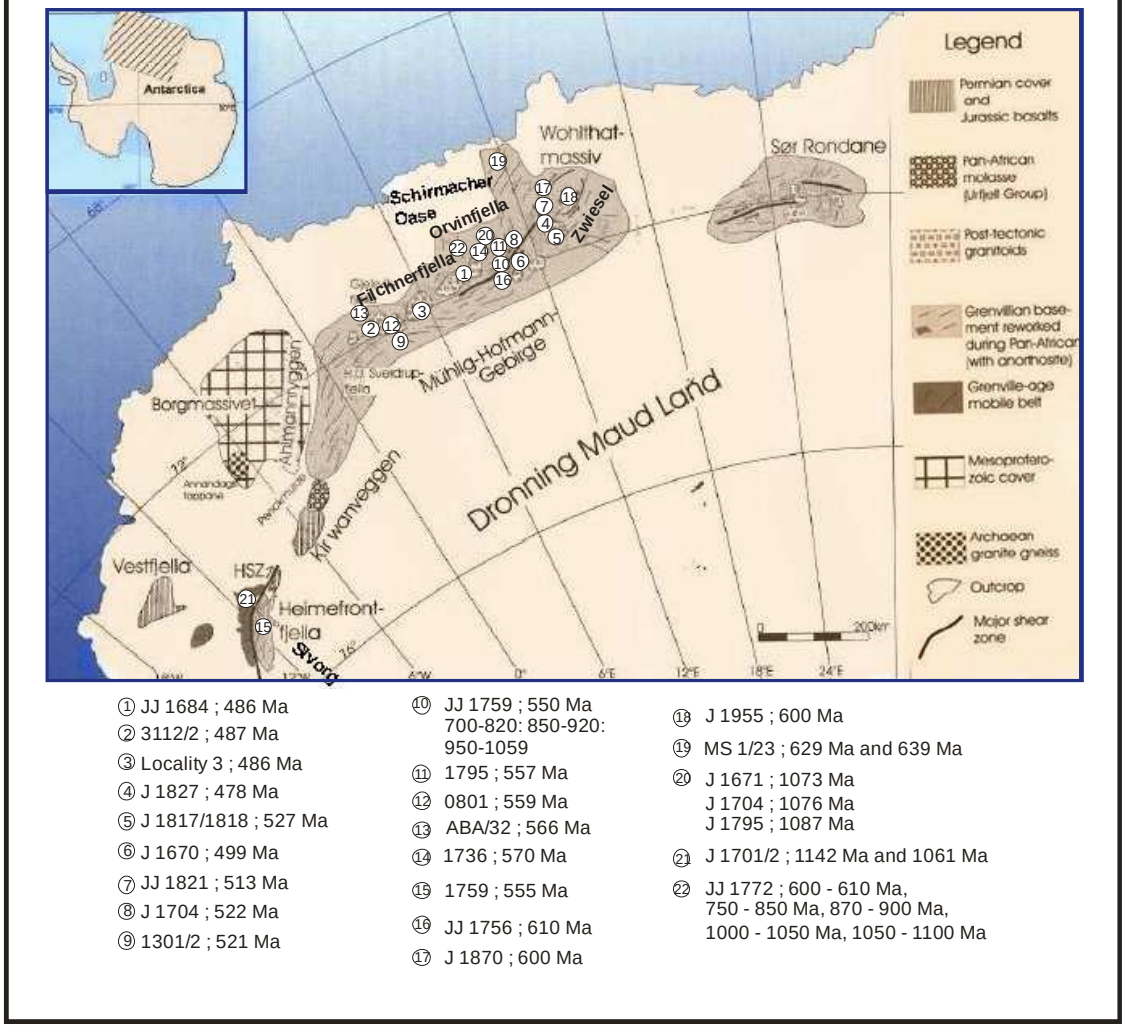

① JJ 1684 ; 486 Ma
② 3112/2 ; 487 Ma
③ Locality 3 ; 486 Ma
④ J 1827 ; 478 Ma
⑤ J 1817/1818 ; 527 Ma
⑥ J 1670 ; 499 Ma
⑦ JJ 1821 ; 513 Ma
⑧ J 1704 ; 522 Ma
⑨ 1301/2 ; 521 Ma
⑩ JJ 1759 ; 550 Ma
700-820: 850-920: 950-1059
⑪ 1795 ; 557 Ma
⑫ 0801 ; 559 Ma
⑬ ABA/32 ; 566 Ma
⑭ 1736 ; 570 Ma
⑮ 1759 ; 555 Ma
⑯ JJ 1756 ; 610 Ma
⑰ J 1870 ; 600 Ma
⑱ J 1955 ; 600 Ma
⑲ MS 1/23 ; 629 Ma and 639 Ma
⑳ J 1671 ; 1073 Ma
J 1704 ; 1076 Ma
J 1795 ; 1087 Ma
㉑ J 1701/2 ; 1142 Ma and 1061 Ma
㉒ JJ 1772 ; 600 - 610 Ma,
750 - 850 Ma, 870 - 900 Ma,
1000 - 1050 Ma, 1050 - 1100 Ma

Fig. 25: Geological map of Dronning Maud Land, East Antarctica, showing the location of the samples of this study and the some samples of the previous study, modify from Bauer et al. (2003).

6. **Discussion**

All of the six analyzed samples with LA-ICPMS method showed similar distribution with majority of ages range between 1100 Ma to 910 Ma, 900 Ma to 620 Ma, 610 Ma to 535 Ma, 530 Ma to 458 Ma (Fig. 26). However, the small variations among the samples of zircons detritus are almost certain, but there were some differences in the number of analyzed grains and their quality. The oldest ages of 1100 Ma to 910 Ma correspond with the Rodinia formation (Fig. 27). The age of 900 Ma to 620 Ma occurrence is due to the number of rifting associated with the destruction of Rodinia (Fig. 27 & 28). The ages of 610 Ma to 535 Ma can corresponds with the supercontinent Gondwana assembly (Fig. 28). The youngest age of 530 Ma to 458 Ma corresponds with the final stage of Gondwana assembly (Fig. 29). Most of these results reasonable well agree with the chronology of supercontinent Gondwana assembly in the cDML.

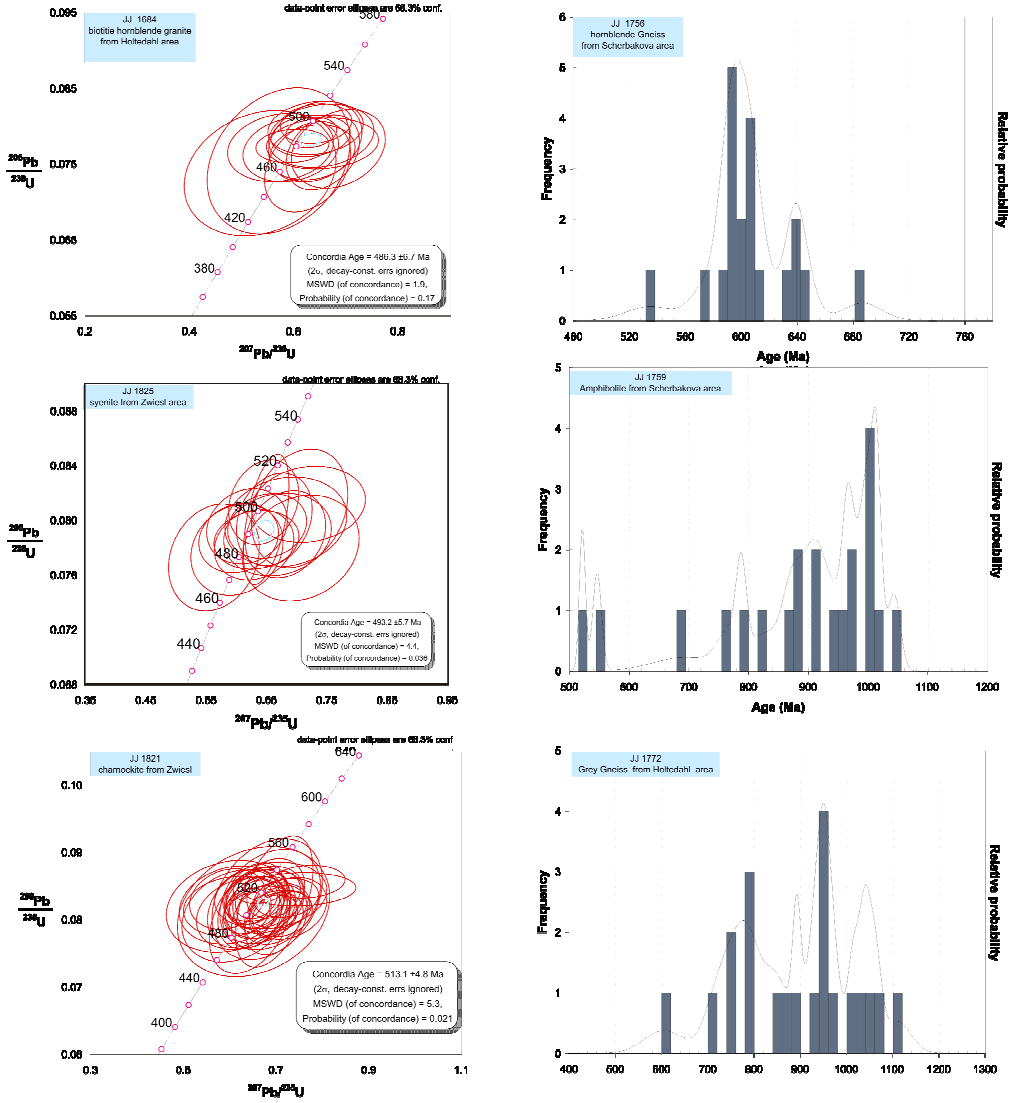

Fig. 26: Majority of Samples age's distribution in central Dronning Maud Land, results are from the present study.

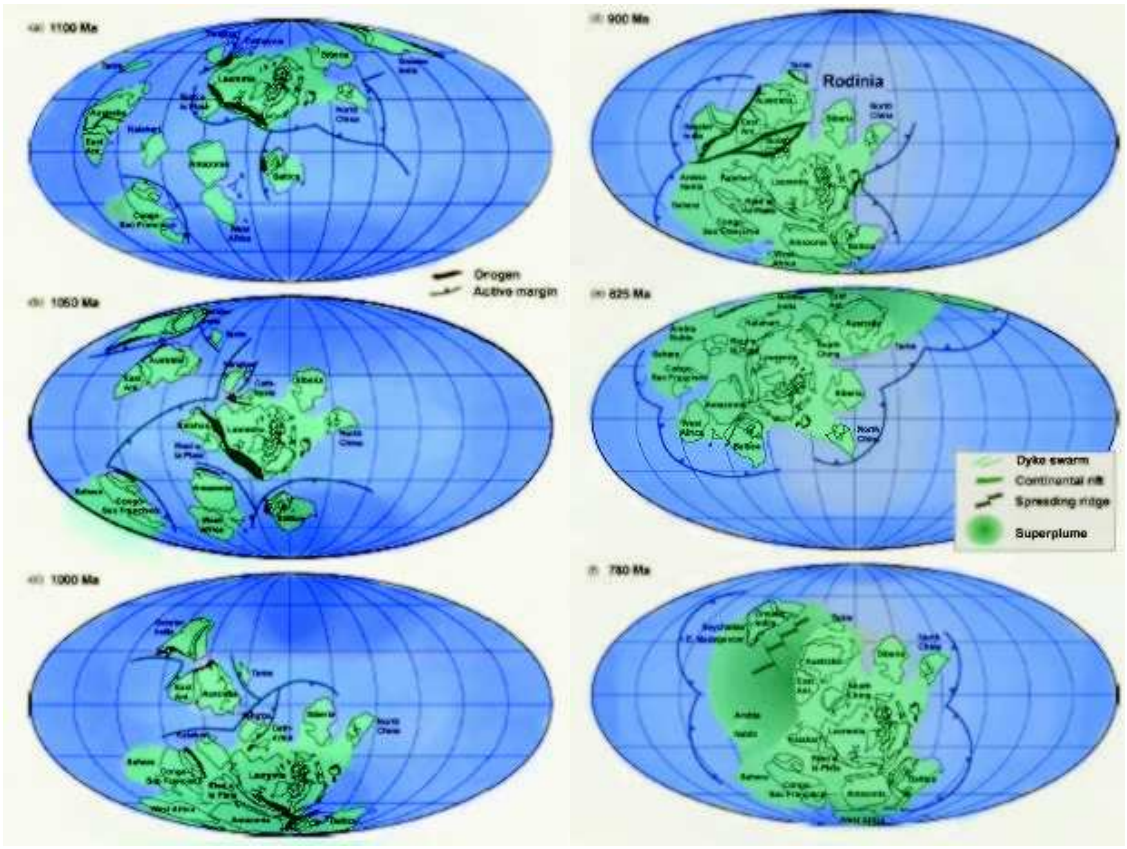

Fig. 27: destruction of Rodinia between 1100 Ma to 1000 Ma in the right side. In the left side shows when the Rodinia start destruction from 900 Ma, modify from Li et al. (2008).

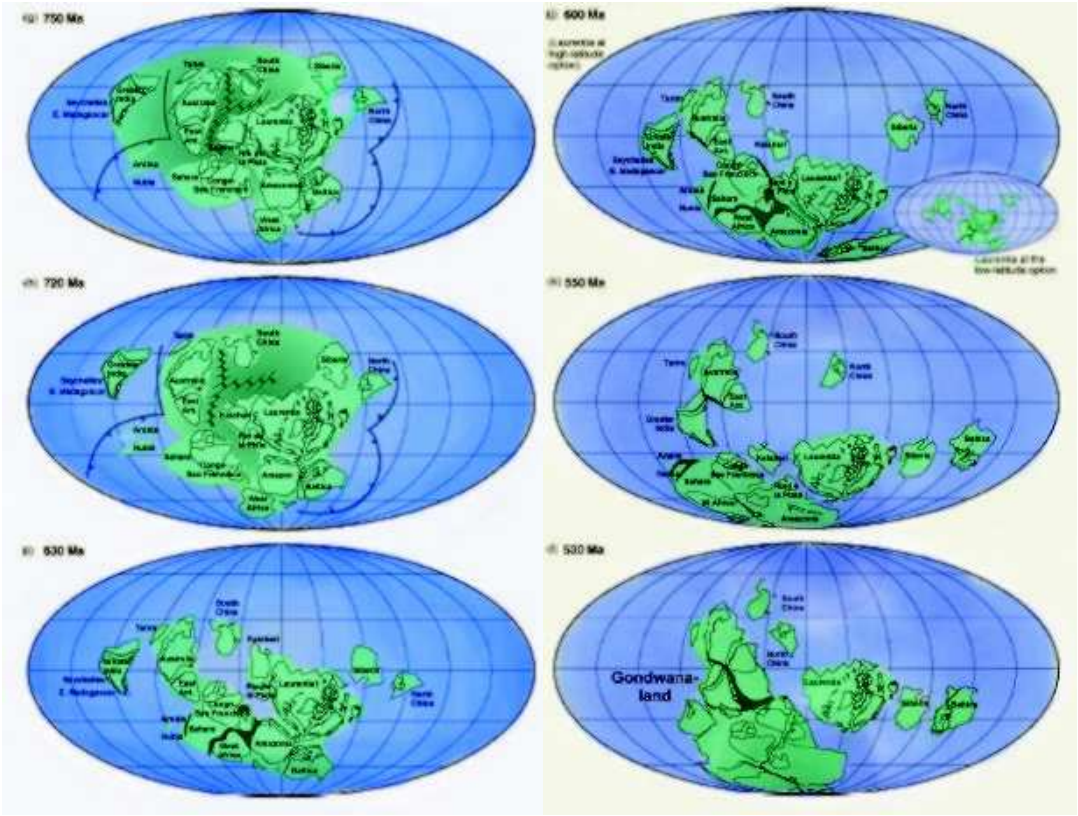

Fig. 28: Shows the several step of rifting during destruction of Rodinia in the left side. In the right side, shows that Gondwana assemblage starts from 600 Ma modify from Li et al. (2008).

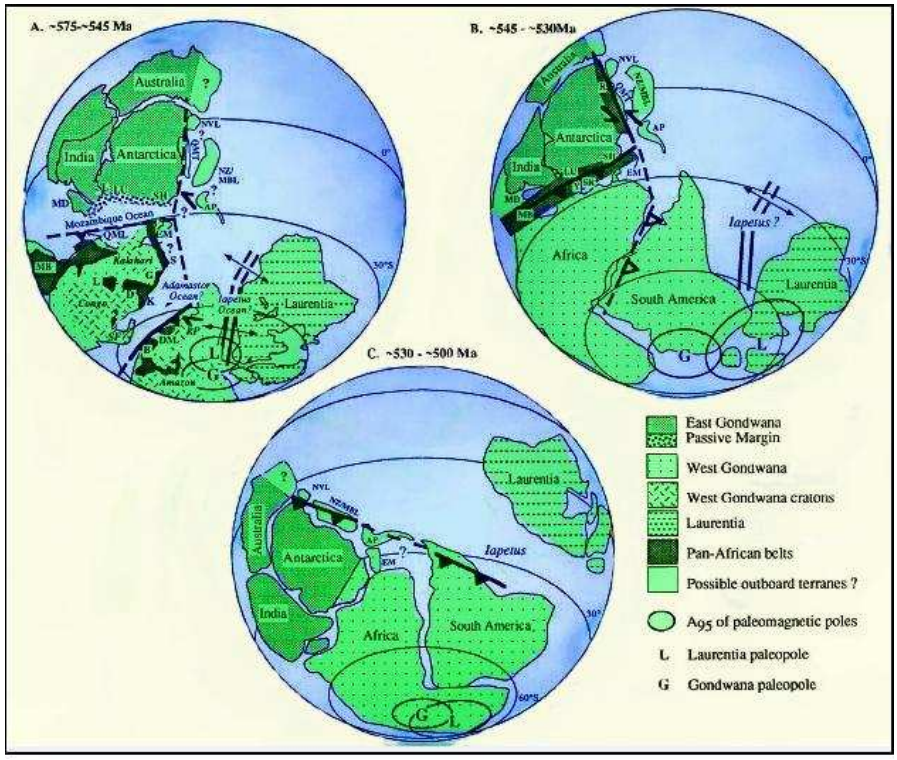

Fig. 29: after the supercontinent Gondwana assemblages took place, final stage of Gondwana assembly from 530 Ma to 500 Ma. Modify from Grunow et al. (1996)

7. Conclusion

1. Data presented in this work brings out a different thermal history for the central Dronning Maud Land.

2. The structure of major shear zones were not investigated in the present study, however, voluminous late tectonic intrusions in central Dronning Maud Land seem to be related to theses structures result of the collapse and extension association.

3. The juvenile ages are not recognized in this study.

4. The setting of the central Dronning Maud Land from this study can be summarized as follows:

a) Metamorphism following by magmatic phase during Rodinia formation,

b) Metamorphism phase intrude by magmatic intrusion among destruction of Rodinia, and

c) Gondwana assemblage of:

- Granulite facies and the amphibolite facies then followed with granitoid intrusion, associated with collision-collision during supercontinent during Pan-Africana I.
- High grade metamorphism and the magmatic intrusion during Pan-Africana II that is related to the collapse and extension during supercontinent.

5. The granitoids intrusions results from the delamination of the root of the lithosphere, following by extension among the crust.

6. The continuity of Mozambique Belt southward into East Antarctica in central Dronning Maud Land

Reference

Abdelsalam, M. G., Liégeois, J. P. & Stern, R. J. 2002. The Saharan Metacraton. *Journal of African Earth Sciences*, 34, 119-136.

Avigad, D., Kolodner, K., McWilliams, M., Persing, H. & Weissbrod, T. 2003. Origin of northern Gondwana Cambrian sandstone revealed by detrital zircon SHRIMP dating *Geology*, 31, 227-230.

Bauer, W., Jacobs, J. & Paesh, H.-J. 2004. Structural evolution of the crystalline basement of central Dronning Maud Land, East Antarctica *Geologisches Jahrbuch,Reihe B*, 96, 325-363.

Bauer, W., Thomas, R. J. & Jacobs, J. 2003. Proterozoic-Cambrian history of Dronning Maud Land in the context of Gondwana assembly. *Geological Society, London, Special Publications*, 206, 247.

Bingen, B., Boyd, R. & Thomas, R. J. 2006b. Crustal architecture in Northern Mozambique: results from a regional bedrock mapping project. In: EGU General Assembly, Vienna. *Geophysical Research Abstracts*, 8

Bingen, B., Jacobs, J., Viola, G., Henderson, I. H. C., Skår, Ø., Boyd, R., Thomas, R. J., Solli, A., Key, R. M. & Daudi, E. X. F. 2009. Geochronology of the Precambrian crust in the Mozambique belt in NE Mozambique, and implications for Gondwana assembly. *Precambrian Research*, 170, 231-255.

Bingen, B., Viola, G., Henderson, I. H. C. & Fanning, C. M. 2006a. Geochronology of Pan-African terrain assembly in the NE Mozambique. In: 21st Colloquium of African Geology, Maputo *Mozambique. Abstract*, 12-14.

Bisnath, A., Frimmel, H. E., Armstrong, R. A. & Board, W. S. 2006. Tectono-thermal evolution of the Maud Belt: New SHRIMP U-Pb zircon data from Gjelsvikfjella, Dronning Maud Land, East Antarctica. *Precambrian Research*, 150, 95-121.

Board, W. S., Frimmel, H. E. & Armstrong, R. A. 2005. Pan-African tectonism in the Western Maud Belt: P-T-t path for high-grade gneisses in the HU Sverdrupfjella, East Antarctica. *Journal of Petrology*, 46, 671-699.

Bohrmann, P. & Fritzsche, D. 1995. The Schirmacher Oasis, Queen Maud Land, East Antarctica and its surroundings. *Petermanns Geograph Mitt Ergänzungsheft*, 289.

Bucher, K. & Frost, B. R. 1995. Charnockites and granulites of the Thor Range, Queen Maud Land, Antarctica-water recycling in high-grade metamorphism. *Terra Abstracts*, 7, 314.

Burke, K. & Kraus, J. U. 2000. Deposition of immense Cambro-Ordovician sandstone bodies, now exposed mainly in N. Africa and Arabia, during the aftermath of the final assembly of Gondwana. *Geological Society of America Abstracts with Program*, 32, 249.

D'Souza, M. J., Kundu, A. & Kaul, M. K. 1996. The geology of central Dronning Maud Land (cDML), East Antarctica. *Ind Min*, 50, 323-338.

Dunstan, L. P., Gramlich, J. W., Barnes, I. L. & Purdy, W. C. 1980. Absolute Isotopic Abundance and the Atomic Weight of a Reference Sample of Thallium. *Journal of Research of the National Bureau of Standards*, 85, 1-10.

Eby, G. N. 1992. Chemical subdivision of the A-typeChemical subdivision of the A-type granitoids: petrogenetic and tectonic implications. *Geology*, 20, 641-644.

Engvik, A. K. & Elvevold, S. 2004. Pan-African extension and near-isothermal exhumation of a granulite facies terrain, Dronning Maud Land, Antarctica *Geological Magazine*, 141, 649-660.

Engvik, A. K. & Elvevold, S. 2006. Late Pan'African Fluid Infiltration in the Miihlig'Hofmann'and Filchnerfjella of Central Dronning Maud Land, East Antarctica.

Frost, B. R. & Bucher, K. 1993. Charnockites and granulites of the Thor Range, Queen Maud Land, Antarctica; the granulite uncertainty principle exemplified. *Abstracts, Annual Meeting of the Geological Society of America*, A, 448.

Grantham, G. H., Macey, P. H., Ingram, B. A., Roberts, M. P., Armstrong, R. A., Hokada, T., Shiraishi, K., Jackson, C., Bisnath, A. & Manhica, V. 2008. Terrane correlation between Antarctica, Mozambique and Sri Lanka:Comparison of geochronology, lithology, structure and metamorphism and possible implications for the geology of southern Africa and Antarctica. In: Satish-Kumar, M., Motoyoshi, Y., Osanai, Y., Hiroi, Y., Shiraishi, K. (Eds.), Geodynamic Evolution of East Antarctica: A Key to the East-West Gondwana Connection. *Geological Society of London, Special Publications*, 308, 91-119.

Grunow, A., Hanson, R. & Wilson, T. 1996. Were aspects of Pan-African deformation linked to Iapetus opening? *Geological Magazine*, 24, 1063.

Henjes-Kunst, F. 2004. Further evidence for Pan-African magmatism and metamorphism in Central Dronning Maud Land, East Antarctica, from rocks at Schirmacheroase: a geochronological study *Geologisches Jahrbuch, Reihe B*, 96, 255-292.

Horn, I., Rudnick, R. L. & McDonough, W. F. 2000. Precise elemental and isotope ratio determination by simultaneous solution nebulization and laser ablation-ICP-MS: application to U-Pb geochronology. *Chemical Geology*, 164, 281-301.

Jackson, S. E., Pearson, N. J., Griffin, W. L. & Belousova, E. A. 2004. The application of laser ablation-inductively coupled plasma-mass spectrometry to in situ U-Pb zircon geochronology. *Chemical Geology*, 211, 47-69.

Jacobs, J., Bauer, W. & Fanning, C. M. 2003b (New). New age constraints for Grenville-age metamorphismin western central Dronning Maud Land (East Antarctica), and implications for the palaeogeography of Kalahari in Rodinia. *International Journal of Earth Sciences*, 92, 302-315.

Jacobs, J., Bauer, W. & Fanning, C. M. 2003a-a. Late Neoproterozoic/Early Palaeozoic events in central Dronning Maud Land and significance for the southern extension of East African Orogen into East Antarctica. *Precambrian Research*, 126, 27-53.

Jacobs, J., Baur, W., Fanning, C. M., & Etal 2003a-b. Late Neoproterozoic/Early Palaeozoic events in central Dronning Maud Land and significance for the southern extension of the East African Orogen into East Antarctica. *Precambrian Research*, 126, 27-53.

Jacobs, J., Bingen, B., Thomas, R. J., Bauer, W., Wingate, M. T. D. & Feitio, P. 2008. Early Palaeozoic orogenic collapse and voluminous late-tectonic magmatism in Dronning Maud Land and Mozambique: insights into the partially delaminated orogenic root of the East African Antarctic Orogen? *Geological Society, London, Special Publications*, 308, 69-90.

Jacobs, J., Fanning, C. M. & Bauer, W. 2003a (Timing). Timing of Grenville-age vs. Pan-African medium-to high grade metamorphism in western Dronning Maud

Land (East Antarctica) and significance for correlations in Rodinia and Gondwana. *Precambrian Research*, 125, 1-20.

Jacobs, J., Fanning, C. M., Henjes-Kunst, F., Olesch, M. & Paech, H. J. 1998. Continuation of the Mozambique Belt into East Antarctica: Grenville-Age metamorphism and polyphase Pan-African high grade events in central Dronning Maud Land. *Journal of Geology*, 106, 385-406.

Jacobs, J., Klemd, R., Fanning, C. M., Bauer, W. & Colombo, F. 2003b. Extensional collapse of the late Neoproterozoic-early Palaeozoic East African-Antarctic Orogen in central Dronning Maud Land, East Antarctica. In:Yoshida, M., Windley, B. F., Dasgupta, S. (Eds.), Proterozoic East Gondwana: Supercontinent Assembly and Breakup. *Geological Society of London, Special Publications*, 206, 271-287.

Jacobs, J. & Thomas, R. J. 2004. Himalayan-type indenter-escape tectonics model for the southern part of the late Neoproterozoic-early Paleozoic East African-Antarctic orogen. *Geology*, 32, 721–724.

John, T., Schenk, V., Mezger, K. & Tembo, F. 2004a. Timing and PT evolution of whiteschist metamorphism in the Lufilian Arc-Zambezi Belt orogen (Zambia): implications for the assembly of Gondwana. *The Journal of geology*, 112, 71-90.

John, T., Scherer, E. E., Haase, K. & Schenk, V. 2004b. Trace element fractionation during fluid-induced eclogitization in a subducting slab: trace element and Lu-Hf-Sm-Nd isotope systematics. *Earth and Planetary Science Letters*, 227, 441-456.

Johnson, P. R. & Woldehaimanot, B. 2003. Development of the Arabian-Nubian Shield: perspectives on accretion and deformation in the northern East African Orogen and the assembly of Gondwana. *Geological Society, London, Special Publications*, 206, 289.

Joshi, A., Pant, N. C. & Parimoo, M. L. 1991. Granites of Petermann ranges, east Antarctica and implication on their genesis. *J Geo Soc Ind*, 38, 169-181.

Kamenev, E. N., Kamenev, A. G. I. a. K., V. P., & Etai 1990. Zemlya Korolevy Maud, In Ivanov, V. L., and Kamenev, E. N., eds., . *Geologiya i Mineralnye Resursy Antarktidy: Moskva*, 113-147.

Kennedy, W. Q. 1964. The structural differentiation of Africa in the Pan-African (±500 my) tectonic episode *Leeds University Research Institute for African Geology Annual Report*, 8, 48-49.

Klimov, L. V., Ravich, M. G. & Soloviev, D. S. 1964. Charnockites of EastAntarctica. In:Adie, R. J. (ed.) Antarctic Geology. North Holland *Amsterdam*, 455-462.

Kosler, J., Fonneland, H., Sylvester, P., Tubrett, M. & Pedersen, R. B. 2002. U-Pb dating of detrital zircons for sediment provenance studies - a comparison of laser ablation ICPMS and SIMS techniques. *Chemical Geology*, 182, 605-618.

Kosler, J. & Sylvester, P. J. 2003. Present trends and the future of zircon in geochronology: laser ablation ICPMS. *Reviews in mineralogy and geochemistry*, 53, 243.

Kröner, A. 2001. The Mozambique belt of East Africa and Madagascar; significance of zircon and Nd model ages for Rodinia and Gondwana supercontinent formation and dispersal *South African Journal of Geology*, 104, 151-166.

Kröner, A., Sacchi, R., Jaeckel, P. & Costa, M. 1997. Kibaran magmatism and Pan-African granulite metamorphism in northern Mozambique: Single zircon ages and regional implications. *Journal of African Earth Sciences*, 25, 467-484.

Kröner, A. & Stern, R. J. 2005. Pan-African Orogeny North African Phanerozoic Rift Valley. *Encyclopedia Of Geology*, 1.

Li, Z. X., Bogdanova, S. V., Collins, A. S., Davidson, A., De Waele, B., Ernst, R. E., Fitzsimons, I. C. W., Fuck, R. A., Gladkochub, D. P., Jacobs, J., Karlstrom, K. E., Lu, S., Natapov, L. M., Pease, V., Pisarevsky, S. A., Thrane, K. & Vernikovsky, V. 2008. Assembly, configuration, and break-up history of Rodinia: A synthesis. *Precambrian Research*, 160, 179-210.

Ludwig, K. R. 1999. IsoplotEx v2.6. Berkeley Geochronology Center Special Publications la. 1-50.

Macey, P. H., Ingram, B., Cronwright, M., Botha, G., Roberts, M., Grantham, G., Maree, L., Botha, P., Kota, M., Opperman, R., Haddon, I. G., Rowher, M. & Nolte, J. C. 2007. Map Explanation of Sheets Alto Molócuè (1537). *Murrupula (1538), Nampula (1639), Mogincual (1540), Errego (1637), Gile (1638) and Angoche (1639-40): Maputo, National Directorate of Geology, Mozambique*, 402.

Macey, P. H., Thomas, R. J., Grantham, G. H., Ingram, B. A., Jacobs, J., Armstrong, R. A., Roberts, M. P., Bingen, B., Hollick, L., de Kock, G. S., Viola, G., Bauer, W., Gonzales, E., Bjerkgard, T., Henderson, I. H. C., Sandstad, J. S., Cronwright, M. S., Harley, S., Solli, A., Nordgulen, O., Motuza, G., Daudi, E. & Manhica, V. 2010. Mesoproterozoic geology of the Nampula Block, northern Mozambique: Tracing fragments of Mesoproterozoic crust in the heart of Gondwana. *Precambrian Research*, 182, 124-148.

Markl, G., Abart, R., Vennemann, T. & Sommer, H. 2003. Mid-crustal metasomatic reaction veins in a spinel peridotite. *J Petrol*, 44, 1097-1120.

Markl, G. & Henjes-Kunst, F. 2004. Magmatic conditions of formation and autometasomatism of post-kinematic charnockites in central Dronning Maud Land, East Antarctica: a model of magmatic evolution. *GEOLOGISCHES JAHRBUCH REIHE B*, 96, 139.

Meier, S. 1999. Paleozoic and Mesozoic tectono-ermal history of central Dronning Maud Land, East Antarctica - evidence from fission-track thermochronology. *Polarforsc*, 337, 192.

Mikhalsky, E. V., Beliatsky, B. V., Savva, E. V., Wetzel, H. U., Fedorov, L. V., Weiser, T. & Hahne, K. 1997. Reconnaissance geochronologic data on polymetamorphic and igneous rocks of the Humboldt Mountains, Central Queen Maud Kand, East Antarctica, in the Antarctic region: Geological evolution and processes, edited by C.A. Ricci *Terra Antarctica Publication, Siena*, 45-54.

Muhongo, S. & Lenoir, J.-L. 1994. Pan-African granulite-facies metamorphism in the Mozambique belt of Tanzania: U-Pb zircon geochronology. *Journal of the Geological Society, London*, 151, 343–347.

Norconsult Consortium 2007. Mineral Resources Management Capacity Building Project, Republic of Mozambique; Component 2: Geological Infrastructure Development Project,Geological Mapping Lot 1; Sheet Explanation: 32 Sheets; Scale: 1/250000, Report No. B6.f. Tech. rep.,. *Republic of Mozambique.*

Ohta, Y., Tørudbakken, B. & Shiraishi, K. 1990. Geology of Gjelsvikfjella and western Mühlig-Hofmannfjella, Dronning Maud Land, east Antarctica. *Polar Research*, 8, 99-129.

Paulsson, O. & Austrheim, H. 2003. A geochronological and geochemical study of rocks from Gjelsvikfjella, Dronning Maud Land,Antarctica – implications for Mesoproterozoic.

Pinna, P., Jourde, G., Calvez, J. Y., Mroz, J. P. & Marques, J. M. 1993. The Mozambique Belt in northern Mozambique; Neoproterozoic (1100 - 850 Ma) crustal growth and tectogenesis, and superimposed Pan-African (800 - 550 Ma) tectonism. *Precambrian Research*, 62, 1-59.

Ravich, M. G. & Kamenev, E. N. 1972. Kristallicheskiy fundament arkticheskoj plartformy (The crystalline basement of the Antarctic platform), Gidrometeoizdat, Leningrad, 658 p (russ.) (Translation Crystalline basement of the Antarctic platform). *Jerusalem*, 1975, 574p.

Ravich, M. G. & Solov'ev, D. S. 1966. Geologiya i petrologiya tsentral'noy chasti gor zemli Korelevy Mod (Geology and petrology of the central Dronning Maud Land): Nedra, Leningrad, . 289p.

Ravikant, V., Laux, J. H. & Pimentel, M. M. 2007. Sm--Nd and U--Pb isotopic constraints for crustal evolution during Late Neoproterozoic from rocks of the Schirmacher Oasis, East Antarctica: geodynamic development coeval with the East African Orogeny. *US Geological Survey, Open-File Report*, 1047.

Roland, N. W. 2002. Pan-African granitoids in central Dronning Maud Land, East Antarctica: Petrography, geochemistry, and plate tectonic setting. *Antarctica at the close of a millennium: Royal Society of New Zealand Bulletin*, 15, 85-91.

Sláma, J., Kosler, J., Condon, D. J., Crowley, J. L., Gerdes, A., Hanchar, J. M., Horstwood, M. S. A., Morris, G. A., Nasdala, L., Norberg, N., Schaltegger, U., Schoene, B., Tubrett, M. N. & Whitehouse, M. J. 2008. Plesovice zircon - A new natural reference material for U-Pb and Hf isotopic microanalysis. *Chemical Geology*, 249, 1-35.

Stern, R. J. 1994. Arc assembly and continental collision in themNeoproterozoic East African Orogen: Implications for the consolidation of Gondwana. *Rev. Earth Planet*, Sci.,22, 31 39-351.

Ueda, k. 2011. Orogenic decay from collision to rifting – characteristics and implications of delamination illustrated by a case study of the East African-Antarctic Orogen in NE Mozambique. *Earth Science.* University of Bergen, Norway.

Viola, G., Henderson, I. H. C., Bingen, B., Thomas, R. J., Smethurst, M. A. & deAzavedo, S. 2008. Growth and collapse of a deeply eroded orogen: insights from structural and geochronological constraints on the Pan-African evolution of NE Mozambique. Tectonics 27.

Wiedenbeck, M., Alle, P., Corfu, F., Griffin, W. L., Meier, M., Oberli, F., Quadt, A., R, oddick, J. C. & Spiegel, W. 1995. Three natural zircon standards for U-Th-Pb, Lu-Hf, trace element and REE analyses. *Geostandards and Geoanalytical Research*, 19, 1-23.

APPENDIX

Table. 3 Analytical results JJ1684

	ISOTOPIC RATIOS						CALCULATED AGES (Ma)					
Analysis	$^{207}Pb/^{235}U$	± 1 sigma	$^{206}Pb/^{238}U$	± 1 sigma	$^{207}Pb/^{206}Pb$	± 1 sigma	$^{207}Pb/^{235}U$	± 1 sigma	$^{206}Pb/^{238}U$	± 1 sigma	$^{207}Pb/^{206}Pb$	± 1 sigma
1	0.6544	0.0708	0.0777	0.0022	0.06109	0.005924	511.2	43.5	482.3	13.3	642.4	208.5
2	0.6331	0.0322	0.0792	0.0013	0.058008	0.003127	498.0	20.0	491.1	7.9	530.1	118.1
3	0.6405	0.0589	0.0779	0.0035	0.059614	0.004799	502.6	36.4	483.7	21.0	589.6	174.6
~~4~~	~~0.7329~~	~~0.1207~~	~~0.0752~~	~~0.0033~~	~~0.070727~~	~~0.012627~~	~~558.3~~	~~70.7~~	~~467.2~~	~~19.6~~	~~949.5~~	~~365.4~~
~~5~~	~~0.5351~~	~~0.0959~~	~~0.0738~~	~~0.0055~~	~~0.052607~~	~~0.009782~~	~~435.2~~	~~63.4~~	~~458.8~~	~~32.7~~	~~311.9~~	~~423.2~~
6	0.6847	0.0593	0.0770	0.0034	0.064515	0.00605	529.6	35.7	478.0	20.4	758.6	197.8
7	0.5741	0.0668	0.0772	0.0030	0.05397	0.007052	460.7	43.1	479.1	17.8	369.8	294.3
8	0.6049	0.1063	0.0601	0.0036	0.072963	0.013007	480.3	67.3	376.4	22.2	1012.9	361.3
9	0.5938	0.0604	0.0769	0.0028	0.056016	0.005705	473.3	38.5	477.5	16.8	453.0	226.1
10	0.6350	0.0539	0.0765	0.0024	0.060196	0.005247	499.2	33.5	475.3	14.4	610.6	188.4
~~11~~	~~0.5856~~	~~0.1043~~	~~0.0794~~	~~0.0026~~	~~0.053505~~	~~0.008519~~	~~468.0~~	~~66.8~~	~~492.4~~	~~15.7~~	~~350.3~~	~~359.9~~
12	0.5705	0.0902	0.0754	0.0064	0.054884	0.006825	458.4	58.3	468.6	38.1	407.5	278.3
13	0.6318	0.0501	0.0787	0.0018	0.05822	0.004803	497.2	31.2	488.4	10.8	538.0	180.5
14	0.6421	0.0452	0.0803	0.0017	0.057981	0.00418	503.6	28.0	498.0	10.3	529.0	158.0
15	0.6259	0.0542	0.0746	0.0039	0.060825	0.005329	493.5	33.9	464.0	23.6	633.1	188.6
16	0.6549	0.0464	0.0765	0.0033	0.062078	0.005786	511.5	28.4	475.3	19.6	676.8	199.2
17	0.6412	0.0602	0.0797	0.0023	0.058322	0.005328	503.0	37.3	494.5	13.9	541.9	199.8
18	0.5969	0.0462	0.0774	0.0015	0.055955	0.004758	475.3	29.3	480.4	8.8	450.6	188.9
19	0.6519	0.0665	0.0787	0.0028	0.060072	0.005703	509.6	40.9	488.4	16.5	606.2	205.3

The data with strikethrough are being rejected

APPENDIX

Table. 4 Analytical results JJ1825

Analysis	ISOTOPIC RATIOS						CALCULATED AGES (Ma)					
	$^{207}Pb/^{235}U$	± 1 sigma	$^{206}Pb/^{238}U$	± 1 sigma	$^{207}Pb/^{206}Pb$	± 1 sigma	$^{207}Pb/^{235}U$	± 1 sigma	$^{206}Pb/^{238}U$	± 1 sigma	$^{207}Pb/^{206}Pb$	± 1 sigma
1	0.6684	0.0586	0.0790	0.0020	0.061391	0.005774	519.7	35.7	489.9	11.9	653.0	201.8
2	0.6630	0.0412	0.0801	0.0022	0.060061	0.004155	516.5	25.2	496.5	13.4	605.8	149.6
3	0.6041	0.0435	0.0787	0.0017	0.055669	0.004382	479.9	27.5	488.4	10.0	439.2	175.2
4	0.6180	0.0440	0.0796	0.0018	0.056342	0.003594	488.6	27.6	493.4	10.9	465.9	141.3
5	0.6496	0.0249	0.0801	0.0031	0.05885	0.001947	508.2	15.3	496.5	18.8	561.6	72.1
6	0.6335	0.0463	0.0786	0.0014	0.058478	0.004451	498.3	28.8	487.6	8.5	547.7	166.3
~~7~~	~~40.2080~~	~~2.9277~~	~~0.4077~~	~~0.0249~~	~~0.715266~~	~~0.044806~~	~~3775.8~~	~~72.1~~	~~2204.4~~	~~113.8~~	~~4761.7~~	~~89.9~~
8	0.6297	0.0434	0.0782	0.0017	0.058399	0.004126	495.9	27.0	485.4	10.2	544.7	154.4
9	0.6512	0.0430	0.0796	0.0016	0.059352	0.004076	509.2	26.5	493.6	9.3	580.0	149.2
~~10~~	~~0.4501~~	~~0.2268~~	~~0.0777~~	~~0.0038~~	~~0.041993~~	~~0.015799~~	~~377.4~~	~~158.8~~	~~482.6~~	~~22.7~~	~~-226.9~~	~~947.7~~
11	0.6455	0.0382	0.0813	0.0020	0.057572	0.003372	505.7	23.6	504.0	12.2	513.5	128.7
12	0.7194	0.0621	0.0812	0.0018	0.064288	0.005098	550.3	36.6	503.1	11.0	751.1	167.5
13	0.6821	0.0665	0.0799	0.0022	0.061937	0.005553	528.0	40.1	495.4	13.0	671.9	191.8
~~14~~	~~0.6857~~	~~0.0628~~	~~0.0202~~	~~0.0009~~	~~0.245802~~	~~0.021034~~	~~530.2~~	~~37.8~~	~~129.1~~	~~5.6~~	~~3157.9~~	~~135.8~~
15	0.7049	0.0525	0.0809	0.0029	0.063226	0.004937	541.7	31.3	501.3	17.1	715.8	165.9
~~16~~	~~0.5665~~	~~0.0926~~	~~0.0772~~	~~0.0049~~	~~0.053227~~	~~0.007808~~	~~455.7~~	~~60.0~~	~~479.3~~	~~29.3~~	~~338.5~~	~~332.3~~
17	0.7067	0.0636	0.0780	0.0026	0.065742	0.006196	542.8	37.9	484.0	15.3	798.2	197.5
18	0.6013	0.0503	0.0778	0.0022	0.056026	0.003824	478.1	31.9	483.3	13.2	453.4	151.5
19	0.6816	0.0437	0.0790	0.0021	0.062597	0.004752	527.7	26.4	490.0	12.6	694.6	161.8
20	0.5633	0.0495	0.0773	0.0026	0.052869	0.004373	453.7	32.2	479.8	15.4	323.2	187.9

The data with strikethrough are being rejected

APPENDIX

Table. 5 Analytical results JJ1821

Analysis	ISOTOPIC RATIOS						CALCULATED AGES (Ma)					
	$^{207}Pb/^{235}U$	± 1 sigma	$^{206}Pb/^{238}U$	± 1 sigma	$^{207}Pb/^{206}Pb$	± 1 sigma	$^{207}Pb/^{235}U$	± 1 sigma	$^{206}Pb/^{238}U$	± 1 sigma	$^{207}Pb/^{206}Pb$	± 1 sigma
1	0.6291	0.0661	0.0809	0.0035	0.06	0.005073	495.6	41.2	501.4	21.1	468.9	199.1
2	0.6876	0.0714	0.0830	0.0049	0.06	0.003877	531.4	43.0	513.7	29.3	607.9	139.4
3	0.7515	0.0796	0.0845	0.0016	0.06	0.007244	569.1	46.2	523.0	9.7	758.0	236.9
4	0.7669	0.0539	0.0856	0.0016	0.06	0.004932	578.0	31.0	529.6	9.5	773.1	159.8
5	0.6537	0.0448	0.0831	0.0022	0.06	0.003191	510.8	27.5	514.4	13.1	494.7	123.2
6	0.6941	0.0518	0.0818	0.0024	0.06	0.004751	535.3	31.0	506.8	14.5	658.7	165.5
7	0.5973	0.0880	0.0819	0.0045	0.05	0.004312	475.5	55.9	507.7	26.8	322.8	185.3
8	0.6091	0.0713	0.0820	0.0030	0.05	0.005038	483.0	45.0	507.8	17.7	366.8	210.6
9	0.6757	0.0565	0.0826	0.0035	0.06	0.003915	524.2	34.2	511.5	21.0	579.7	143.3
10	0.6944	0.0343	0.0806	0.0020	0.06	0.003563	535.4	20.6	499.5	12.2	691.4	121.6
11	0.5959	0.0539	0.0831	0.0030	0.05	0.004015	474.6	34.3	514.3	17.7	287.2	176.4
12	0.6444	0.0578	0.0799	0.0052	0.06	0.003178	505.0	35.7	495.4	31.1	548.9	118.6
13	0.6964	0.0550	0.0827	0.0064	0.06	0.003223	536.6	32.9	512.0	38.4	642.9	113.4
14	0.6661	0.0383	0.0849	0.0016	0.06	0.0033	518.3	23.3	525.1	9.8	488.7	127.9
15	0.7224	0.0458	0.0832	0.0019	0.06	0.004823	552.1	27.0	515.3	11.4	707.0	162.9
16	0.6595	0.0391	0.0825	0.0025	0.06	0.003861	514.3	23.9	511.3	15.2	527.8	146.0
17	0.7263	0.0549	0.0817	0.0030	0.06	0.004263	554.4	32.3	506.0	18.1	758.3	139.4
18	0.6886	0.0798	0.0836	0.0033	0.06	0.005271	531.9	48.0	517.4	19.4	594.8	191.1
19	0.6844	0.0511	0.0835	0.0037	0.06	0.003335	529.5	30.8	516.8	21.8	584.2	121.8
20	0.6558	0.0411	0.0839	0.0030	0.06	0.003158	512.0	25.2	519.1	18.0	480.8	123.0
21	0.6663	0.0501	0.0818	0.0031	0.06	0.004508	518.5	30.5	506.8	18.3	570.4	166.0
22	0.6578	0.0298	0.0830	0.0019	0.06	0.002479	513.3	18.3	514.0	11.3	510.3	94.8
23	0.6052	0.0747	0.0822	0.0038	0.05	0.003923	480.5	47.3	509.0	22.8	346.8	166.1
24	0.6745	0.0560	0.0831	0.0029	0.06	0.004335	523.5	34.0	514.6	17.2	562.5	160.4
25	0.6303	0.0512	0.0816	0.0038	0.06	0.003045	496.3	31.9	505.9	22.9	452.1	120.8
26	0.6646	0.0522	0.0807	0.0028	0.06	0.00369	517.4	31.9	500.4	16.9	593.4	133.9
~~27~~	~~0.7003~~	~~0.0442~~	~~0.0799~~	~~0.0034~~	~~0.06~~	~~0.004215~~	~~539.0~~	~~26.4~~	~~495.7~~	~~20.3~~	~~726.5~~	~~140.7~~
28	0.6518	0.1082	0.0812	0.0064	0.06	0.005592	509.6	66.5	503.1	38.0	538.7	210.0
29	0.6952	0.0421	0.0802	0.0025	0.06	0.004232	535.9	25.2	497.0	15.1	705.0	143.2

The data with strikethrough are being rejected

APPENDIX

Table. 5 Analytical results JJ1821 continued

Analysis	ISOTOPIC RATIOS						CALCULATED AGES (Ma)					
	$^{207}Pb/^{235}U$	± 1 sigma	$^{206}Pb/^{238}U$	± 1 sigma	$^{207}Pb/^{206}Pb$	± 1 sigma	$^{207}Pb/^{235}U$	± 1 sigma	$^{206}Pb/^{238}U$	± 1 sigma	$^{207}Pb/^{206}Pb$	± 1 sigma
30	0.6111	0.0748	0.0805	0.0045	0.06	0.004503	484.2	47.2	499.3	26.9	413.6	182.9
31	0.6581	0.0356	0.0802	0.0029	0.06	0.003164	513.4	21.8	497.4	17.2	585.6	115.4
32	0.5841	0.1634	0.0804	0.0072	0.05	0.009263	467.1	104.8	498.5	42.7	315.6	399.8
33	0.7138	0.0426	0.0808	0.0022	0.06	0.003582	547.0	25.2	501.0	13.3	743.6	118.2
34	0.6423	0.0294	0.0816	0.0016	0.06	0.002376	503.7	18.2	505.7	9.4	494.7	91.7
35	0.7078	0.0452	0.0816	0.0019	0.06	0.004202	543.4	26.9	505.4	11.1	706.3	142.0
36	0.6811	0.0783	0.0830	0.0059	0.06	0.004441	527.4	47.3	514.2	35.3	585.4	162.0
37	0.6386	0.0340	0.0813	0.0022	0.06	0.002713	501.4	21.1	503.7	13.4	491.4	105.0
38	0.6504	0.0497	0.0817	0.0040	0.06	0.003354	508.7	30.6	506.0	23.8	520.9	127.4
39	0.6949	0.0380	0.0837	0.0023	0.06	0.003403	535.7	22.7	518.1	13.7	611.8	122.1

The data with strikethrough are being rejected

APPENDIX

Table. 6 Analytical results JJ1756

Analysis	ISOTOPIC RATIOS						CALCULATED AGES Ma					
	$^{207}Pb/^{235}U$	± 1 sigma	$^{206}Pb/^{238}U$	± 1 sigma	$^{207}Pb/^{206}Pb$	± 1 sigma	$^{207}Pb/^{235}U$	± 1 sigma	$^{206}Pb/^{238}U$	± 1 sigma	$^{207}Pb/^{206}Pb$	± 1 sigma
1	0.5018	0.0280	0.0599	0.0036	0.060807	0.001388	412.9	18.9	374.7	22.1	632.4	49.2
2	0.7505	0.0283	0.0936	0.0028	0.05816	0.001727	568.5	16.4	576.7	16.2	535.8	65.0
~~3~~	~~0.8598~~	~~0.0419~~	~~0.1059~~	~~0.0037~~	~~0.058892~~	~~0.002242~~	~~630.0~~	~~22.9~~	~~648.8~~	~~21.5~~	~~563.1~~	~~83.0~~
4	0.8532	0.0282	0.0987	0.0025	0.062705	0.00297	626.4	15.5	606.7	14.5	698.2	100.9
5	0.7392	0.0439	0.0866	0.0058	0.061913	0.00191	561.9	25.6	535.3	34.6	671.1	66.0
6	0.8110	0.0320	0.0962	0.0034	0.061131	0.002361	603.0	18.0	592.2	20.1	643.8	83.0
7	0.8253	0.0328	0.0985	0.0029	0.060775	0.002331	611.0	18.2	605.6	17.2	631.3	82.6
8	0.8579	0.0330	0.0996	0.0031	0.062459	0.002626	628.9	18.0	612.1	18.1	689.9	89.7
9	0.7865	0.0211	0.0957	0.0021	0.059628	0.001515	589.2	12.0	589.0	12.2	590.1	55.1
10	0.8017	0.0309	0.0970	0.0029	0.059925	0.001812	597.8	17.4	597.0	17.2	600.9	65.5
11	0.8218	0.0440	0.0977	0.0046	0.061034	0.002995	609.1	24.5	600.7	26.8	640.4	105.5
12	0.8172	0.0389	0.0974	0.0047	0.060874	0.002054	606.5	21.7	598.9	27.3	634.8	72.6
13	0.8352	0.0323	0.0983	0.0026	0.061592	0.002583	616.5	17.9	604.7	15.5	660.0	89.9
14	0.8139	0.0275	0.0965	0.0022	0.061143	0.002048	604.7	15.4	594.2	12.9	644.3	72.0
15	0.7745	0.0354	0.0929	0.0035	0.060456	0.003173	582.4	20.3	572.8	20.6	619.9	113.2
16	0.9464	0.0559	0.1124	0.0048	0.061044	0.002586	676.2	29.2	686.9	27.7	640.8	91.1
~~17~~	~~0.5469~~	~~0.1027~~	~~0.0669~~	~~0.0102~~	~~0.059309~~	~~0.002055~~	~~443.0~~	~~67.4~~	~~417.3~~	~~61.5~~	~~578.5~~	~~75.3~~
~~18~~	~~0.7037~~	~~0.0813~~	~~0.0810~~	~~0.0032~~	~~0.062972~~	~~0.006718~~	~~541.0~~	~~48.4~~	~~502.4~~	~~19.0~~	~~707.3~~	~~226.9~~
19	0.8458	0.0390	0.1042	0.0021	0.058874	0.001397	622.3	21.5	638.9	12.5	562.4	51.7
20	0.8971	0.0423	0.1047	0.0028	0.062142	0.002706	650.2	22.6	641.9	16.5	679.0	93.0
21	0.8885	0.0390	0.1036	0.0028	0.062217	0.003237	645.6	21.0	635.3	16.4	681.6	111.1
22	0.8320	0.0558	0.0961	0.0040	0.062769	0.002537	614.7	30.9	591.7	23.8	700.4	86.1
23	0.8466	0.0650	0.0968	0.0024	0.063401	0.003675	622.8	35.7	595.9	14.2	721.7	123.0
24	0.7725	0.0752	0.0987	0.0043	0.05675	0.003776	581.2	43.1	606.9	25.5	481.8	147.0
25	0.8634	0.0419	0.1051	0.0032	0.059583	0.001933	632.0	22.8	644.2	18.6	588.5	70.4

The data with strikethrough are being rejected

APPENDIX

Table. 7 Analytical results JJ1759 continued

Analysis	ISOTOPIC RATIOS						CALCULATED AGES (Ma)					
	$^{207}Pb/^{235}U$	± 1 sigma	$^{206}Pb/^{238}U$	± 1 sigma	$^{207}Pb/^{206}Pb$	± 1 sigma	$^{207}Pb/^{235}U$	± 1 sigma	$^{206}Pb/^{238}U$	± 1 sigma	$^{207}Pb/^{206}Pb$	± 1 sigma
1	0.6768	0.0317	0.0843	0.0017	0.05822	0.00281	524.8	19.2	521.8	10.2	538.0	105.6
2	1.7891	0.0459	0.1690	0.0050	0.076797	0.001899	1041.5	16.7	1006.4	27.8	1115.9	49.4
3	1.4816	0.0697	0.1451	0.0056	0.074066	0.002184	922.9	28.5	873.4	31.5	1043.3	59.5
4	1.5727	0.0781	0.1530	0.0072	0.074543	0.001924	959.5	30.8	917.8	40.1	1056.2	52.0
5	1.2512	0.0369	0.1299	0.0030	0.069841	0.002101	824.0	16.6	787.5	17.0	923.7	61.8
6	1.3571	0.1124	0.1265	0.0069	0.07781	0.002277	870.6	48.4	767.8	39.6	1142.0	58.2
7	1.6302	0.0470	0.1629	0.0046	0.072601	0.001613	981.9	18.2	972.6	25.2	1002.8	45.1
8	1.6871	0.0543	0.1679	0.0042	0.072885	0.001734	1003.7	20.5	1000.4	23.0	1010.7	48.2
9	1.6803	0.0868	0.1673	0.0057	0.072837	0.011424	1001.1	32.9	997.3	31.3	1009.4	318.1
10	1.7469	0.0503	0.1758	0.0036	0.072072	0.001641	1026.0	18.6	1044.0	20.0	988.0	46.3
11	1.5825	0.0608	0.1570	0.0068	0.073094	0.001621	963.4	23.9	940.2	37.7	1016.6	44.9
12	0.7265	0.0491	0.0885	0.0025	0.059552	0.019875	554.5	28.9	546.5	14.7	587.3	724.1
13	1.3490	0.0808	0.1363	0.0079	0.071754	0.031026	867.1	34.9	824.0	44.8	979.0	881.0
14	1.7640	0.0793	0.1685	0.0060	0.075925	0.003316	1032.3	29.1	1003.9	33.0	1093.1	87.5
15	1.4704	0.0844	0.1476	0.0089	0.072229	0.002603	918.3	34.7	887.7	49.8	992.4	73.3
16	1.5264	0.0537	0.1515	0.0053	0.073088	0.00177	941.1	21.6	909.2	29.9	1016.4	49.0
17	~~2.9670~~	~~0.7670~~	~~0.1477~~	~~0.0108~~	~~0.145709~~	~~0.058172~~	~~1399.2~~	~~196.3~~	~~888.0~~	~~60.5~~	~~2296.2~~	~~686.3~~
18	~~1.0440~~	~~0.2154~~	~~0.1135~~	~~0.0183~~	~~0.066689~~	~~0.001975~~	~~725.9~~	~~107.0~~	~~693.3~~	~~106.1~~	~~828.1~~	~~61.8~~
19	1.5896	0.1038	0.1606	0.0093	0.07177	0.001726	966.1	40.7	960.3	51.8	979.4	49.0
20	1.6430	0.0535	0.1615	0.0031	0.073788	0.001747	986.9	20.6	965.1	17.2	1035.7	47.8
21	1.6101	0.1168	0.1461	0.0093	0.079936	0.013898	974.2	45.4	879.0	52.1	1195.4	343.0
22	1.6997	0.0332	0.1704	0.0024	0.072356	0.001266	1008.4	12.5	1014.2	13.2	996.0	35.6

The data with strikethrough are being rejected

APPENDIX

Table. 8 Analytical results JJ1772

Analysis	ISOTOPIC RATIOS						CALCULATED AGES (Ma)					
	$^{207}Pb/^{235}U$	± 1 sigma	$^{206}Pb/^{238}U$	± 1 sigma	$^{207}Pb/^{206}Pb$	± 1 sigma	$^{207}Pb/^{235}U$	± 1 sigma	$^{206}Pb/^{238}U$	± 1 sigma	$^{207}Pb/^{206}Pb$	± 1 sigma
1	1.8484	0.0627	0.1703	0.0042	0.078725	0.078725	1062.8	22.3	1013.7	23.3	1165.2	348.6
~~2~~	~~2.5111~~	~~0.4194~~	~~0.2144~~	~~0.0232~~	~~0.084958~~	~~0.084958~~	~~1275.3~~	~~121.3~~	~~1252.0~~	~~123.1~~	~~1314.6~~	~~87.3~~
3	1.2960	0.1629	0.1302	0.0158	0.072172	0.072172	844.0	72.1	789.2	90.1	990.8	72.0
4	1.2178	0.1019	0.1245	0.0075	0.070932	0.070932	808.8	46.6	756.5	42.8	955.5	92.5
~~5~~	1.4126	0.0809	0.1300	0.0071	0.078783	0.078783	894.3	34.1	788.1	40.6	1166.7	61.7
6	1.9528	0.1562	0.1747	0.0041	0.081061	0.081061	1099.4	53.7	1038.1	22.6	1222.9	185.1
7	1.1207	0.1020	0.1179	0.0084	0.068967	0.068967	763.3	48.9	718.2	48.3	897.7	229.6
~~8~~	1.5157	0.0889	0.1561	0.0063	0.070415	0.070415	936.7	35.9	935.1	35.4	940.5	66.5
9	1.7098	0.1338	0.1596	0.0084	0.077693	0.077693	1012.2	50.1	954.6	47.0	1139.0	185.0
10	1.6486	0.0722	0.1589	0.0049	0.075236	0.075236	989.0	27.7	950.8	27.1	1074.8	110.3
~~11~~	1.8383	0.0960	0.1755	0.0064	0.07598	0.07598	1059.3	34.3	1042.2	35.0	1094.5	54.0
~~12~~	~~2.3802~~	~~0.4897~~	~~0.1380~~	~~0.0092~~	~~0.125107~~	~~0.125107~~	~~1236.7~~	~~147.1~~	~~833.3~~	~~51.9~~	~~2030.3~~	~~685.8~~
13	1.4070	0.1610	0.1448	0.0137	0.07049	0.07049	891.9	67.9	871.5	77.1	942.7	429.7
~~14~~	~~0.8814~~	~~0.1539~~	~~0.0982~~	~~0.0145~~	~~0.065079~~	~~0.065079~~	~~641.7~~	~~83.1~~	~~604.0~~	~~85.0~~	~~776.9~~	~~92.4~~
15	1.2905	0.1654	0.1307	0.0155	0.071613	0.071613	841.5	73.3	791.8	88.3	975.0	129.0
16	1.7121	0.1616	0.1581	0.0173	0.078522	0.078522	1013.1	60.5	946.4	96.2	1160.1	425.8
~~17~~	~~1.3726~~	~~0.1957~~	~~0.1239~~	~~0.0165~~	~~0.080368~~	~~0.080368~~	~~877.3~~	~~83.7~~	~~752.8~~	~~94.5~~	~~1206.0~~	~~153.9~~
18	1.7236	0.1154	0.1571	0.0080	0.079586	0.079586	1017.4	43.0	940.5	44.5	1186.8	71.7
19	1.4211	0.0907	0.1395	0.0093	0.073903	0.073903	897.8	38.0	841.6	52.6	1038.8	73.8
~~20~~	~~1.8745~~	~~0.0586~~	~~0.1790~~	~~0.0047~~	~~0.075948~~	~~0.075948~~	~~1072.1~~	~~20.7~~	~~1061.5~~	~~25.9~~	~~1093.7~~	~~59.8~~
21	1.8909	0.1269	0.1875	0.0111	0.073154	0.073154	1077.9	44.6	1107.7	60.2	1018.2	58.3
22	1.5911	0.0857	0.1613	0.0064	0.071523	0.071523	966.7	33.6	964.3	35.8	972.4	52.1

The data with strikethrough are being rejected